

Changes in Methionine Metabolism and Histone H3 Trimethylation Are Linked to Mitochondrial Defects in Multiple Sclerosis

Naveen Kumar Singhal,^{1*} Shuo Li,^{1,2*} Erland Arning,⁴ Kholoud Alkhayer,¹ Robert Clements,¹ Zachary Sarcyk,¹ Rohan S. Dassanayake,² Nicola E. Brasch,³ Ernest J. Freeman,¹ Teodoro Bottiglieri,⁴ and Jennifer McDonough¹

Departments of ¹Biological Sciences and ²Chemistry and Biochemistry, Kent State University, Kent, Ohio 44242, ³School of Applied Sciences, Auckland University of Technology, Auckland 1142, New Zealand, and ⁴Institute of Metabolic Disease, Baylor Research Institute, Dallas, Texas 75226

Mitochondrial changes, including decreased expression of electron transport chain subunit genes and impaired energetic, have been reported in multiple sclerosis (MS), but the mechanisms involved in these changes are not clear. To determine whether epigenetic mechanisms are involved, we measured the concentrations of methionine metabolites by liquid chromatography tandem mass spectrometry, histone H3 methylation patterns, and markers of mitochondrial respiration in gray matter from postmortem MS and control cortical samples. We found decreases in respiratory markers as well as decreased concentrations of the methionine metabolites S-adenosylmethionine, betaine, and cystathionine in MS gray matter. We also found expression of the enzyme betaine homocysteine methyltransferase in cortical neurons. This enzyme catalyzes the remethylation of homocysteine to methionine, with betaine as the methyl donor, and has previously been thought to be restricted to liver and kidney in the adult human. Decreases in the concentration of the methyl donor betaine were correlated with decreases in histone H3 trimethylation (H3K4me3) in NeuN+ neuronal nuclei in MS cortex compared with controls. Mechanistic studies demonstrated that H3K4me3 levels and mitochondrial respiration were reduced in SH-SY5Y cells after exposure to the nitric oxide donor sodium nitroprusside, and betaine was able to rescue H3K4me3 levels and respiratory capacity in these cells. Chromatin immunoprecipitation experiments showed that betaine regulates metabolic genes in human SH-SY5Y neuroblastoma cells. These data suggest that changes to methionine metabolism may be mechanistically linked to changes in neuronal energetics in MS cortex.

Key words: betaine; betaine homocysteine methyltransferase; epigenetics; methionine metabolism; mitochondria; multiple sclerosis

Significance Statement

For decades, it has been observed that vitamin B₁₂ deficiency and multiple sclerosis (MS) share certain pathological changes, including conduction disturbances. In the present study, we have found that vitamin B₁₂-dependent methionine metabolism is dysregulated in the MS brain. We found that concentrations of the methyl donor betaine are decreased in MS cortex and are correlated with reduced levels of the histone H3 methyl mark H3K4me3 in neurons. Cell culture and chromatin immunoprecipitation-seq data suggest that these changes may lead to defects in mitochondria and impact neuronal energetics. These data have uncovered a novel pathway linking methionine metabolism with mitochondrial respiration and have important implications for understanding mechanisms involved in neurodegeneration in MS.

Introduction

Multiple sclerosis (MS) is an inflammatory neurodegenerative disease of the CNS, which results in progressive neurological dis-

ability (Bjartmar et al., 2000; Noseworthy et al., 2000). Cortical gray matter pathology, including demyelination, axonal degeneration, and brain atrophy, is recognized as a major factor contributing to disability in MS (Inglese et al., 2004; Bö et al., 2006;

Received Sept. 18, 2014; revised Aug. 22, 2015; accepted Sept. 23, 2015.

Author contributions: J.M. designed research; N.K.S., S.L., E.A., K.A., R.C., Z.S., R.S.D., E.J.F., T.B., and J.M. performed research; N.K.S., S.L., E.A., K.A., R.C., N.E.B., E.J.F., T.B., and J.M. analyzed data; N.K.S., N.E.B., T.B., and J.M. wrote the paper.

This work was supported by the College of Arts and Sciences at Kent State University to J.M. and N.E.B. We thank the Rocky Mountain MS Center (funded by the National Multiple Sclerosis Society) and the Brain and Spinal Cord Resource Center at University of California—Los Angeles for tissue.

The authors declare no competing financial interests.

*N.K.S. and S.L. contributed equally to this work.

Correspondence should be addressed to Dr. Jennifer McDonough, Department of Biological Sciences Kent State University, Kent, OH 44242. E-mail: jmcDonou@kent.edu.

DOI:10.1523/JNEUROSCI.4349-14.2015

Copyright © 2015 the authors 0270-6474/15/3515170-17\$15.00/0

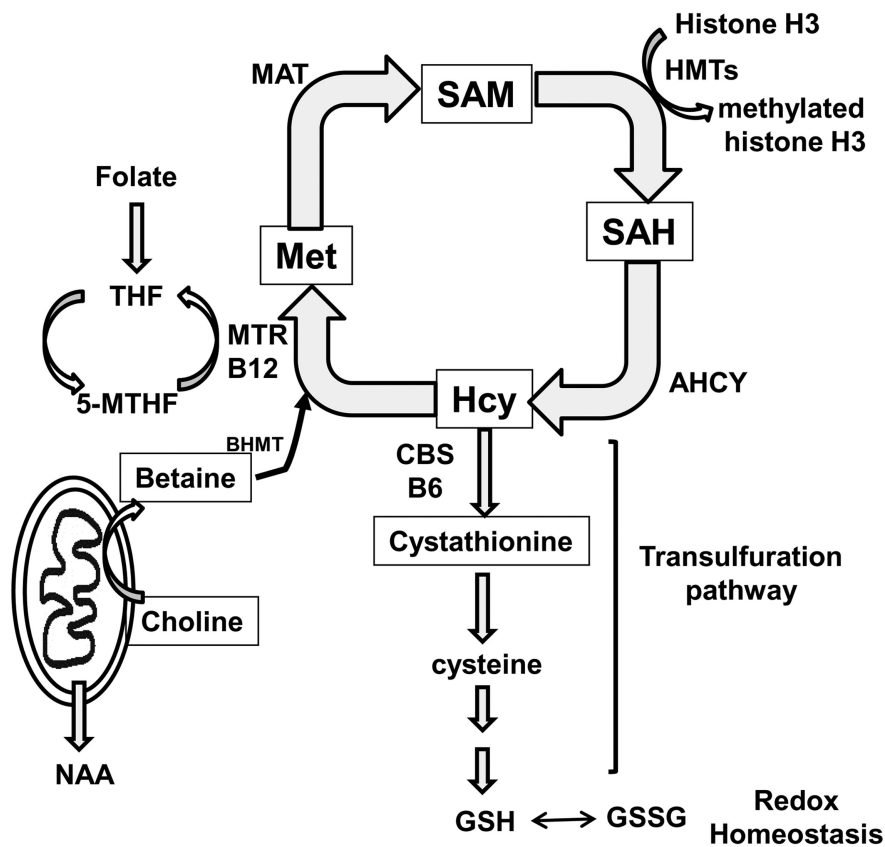


Figure 1. Schematic showing methionine metabolism reactions. The metabolites methionine, SAM, SAH, homocysteine, cystathionine, choline, and betaine were measured by LC-MS/MS. The neuronal mitochondrial metabolite NAA, a marker of neuronal respiratory capacity, was also measured in this study by HPLC. In the methionine cycle, the essential amino acid methionine is converted to SAM by MAT. Upon donating a methyl group, SAM is converted to SAH. SAH is converted to homocysteine by SAH hydrolase (AHCY). Homocysteine is then remethylated to methionine by the B₁₂-dependent enzyme MTR with the methyl group transferred from folate-derived 5-methyltetrahydrofolate (5-MTHF) to B₁₂ (cobalamin) to homocysteine. Betaine can be supplied in the diet or through the oxidation of choline in mitochondria. BHMT catalyzes the conversion of homocysteine to methionine with betaine as the methyl donor. Methylation of histones is catalyzed by histone methyltransferases (HMTs), which transfer a methyl group from SAM to amino acids on histone amino-terminal tails. The methionine cycle is linked to GSH production through the transsulfuration pathway. The first step in this pathway is catalyzed by CBS with vitamin B₆ as a cofactor. GSH is involved in maintaining redox homeostasis in cells. THF, Tetrahydrofolate; GSSG, oxidized glutathione; CBS, cystathionine-β-synthase; MTR, methionine synthase; MAT, methionine adenosyl transferase.

Fisher et al., 2008). Previous studies suggest that mitochondrial defects, including reductions in neuronal expression of nuclear encoded mitochondrial electron transport chain genes, decreased synthesis of the neuronal mitochondrial metabolite *N*-acetylaspartate (NAA), and inhibition of mitochondrial respiration contribute to cortical pathology in MS (Dutta et al., 2006; Pandit et al., 2009; Broadwater et al., 2011; Campbell et al., 2011; Li et al., 2013; Witte et al., 2013); however, the mechanisms involved in these mitochondrial changes are not clear.

A role for epigenetic mechanisms in MS is supported by several studies that identified changes to epigenetic modifications, including histone acetylation and DNA methylation patterns in white matter in MS (Mastrorardi et al., 2007; Pedre et al., 2011; Huynh et al., 2014). Epigenetic modifications mediate changes in chromatin conformation and transcription in response to environmental or physiological signals (Mehler, 2008; Cyr and Domann, 2011). Some of the most prevalent epigenetic modifications involve methylation reactions. In these reactions, DNA and histone methyltransferases catalyze the methylation of amino acids on histone amino-terminal tails and cytosines in DNA with the methyl donor

S-adenosylmethionine (SAM) supplying the methyl group. S-Adenosylhomocysteine (SAH) is the byproduct of all SAM-dependent methylation reactions. SAH is rapidly converted to homocysteine, which is then remethylated to methionine with the methyl group derived from either 5-methyltetrahydrofolate or from betaine. Homocysteine is a branch point metabolite that connects folate metabolism and the methionine cycle to the transsulfuration pathway, which generates the redox regulator glutathione (GSH). A schematic depicting folate, methionine cycle metabolites, enzymes, and related cofactors is shown in Figure 1. Changes in levels of methionine cycle metabolites through dietary restriction of cofactors, such as folate and vitamin B₁₂, in mice has been shown to result in changes in DNA methyltransferase activity that can influence site-specific methylation of promoter regions and gene activity (Fuso et al., 2011a,b).

Historically, it has been noted that there is considerable overlap between the neurological manifestations observed in MS and those of deficiency of the methionine metabolism cofactor vitamin B₁₂, including defects in myelin and conduction abnormalities, suggesting that this metabolic pathway may be dysregulated in MS (Miller et al., 2005). Interestingly, changes in concentrations of methionine, homocysteine, and vitamin B₁₂ have been reported in sera and plasma in subsets of MS patients (Reynolds et al., 1992; Kocer et al., 2009; Zhu et al., 2011; Gardner et al., 2013), but changes in CNS tissue have not been investigated. In the current study, we investigated the relationship between

changes in methionine cycle metabolites, histone H3 methylation, and mitochondria in gray matter from MS and control postmortem cortical tissue samples and in human SH-SY5Y neuroblastoma cells.

Materials and Methods

Postmortem tissue. Postmortem frozen brain tissue was obtained from the Rocky Mountain MS Center and the Brain and Spinal Cord Resource Center at University of California–Los Angeles according to institutional review board protocol. Tissue was matched for brain region, age, and postmortem interval (PMI) as closely as possible. Thirty cortical tissue blocks were obtained from female donor brains and 20 from male donors. Gray and white matter were separated on a cryostat and stored at -80°C . During tissue collection, selected sections from each sample were affixed to microscope slides and immunostained with an antibody to myelin proteolipid protein (PLP) (Millipore) to determine lesion status. Briefly, frozen sections were fixed in 70% ethanol and treated with 1% hydrogen peroxide to quench endogenous peroxidase activity. They were subsequently blocked in 3% donkey serum and incubated with the appropriate antibody diluted 1:200 in PBS containing 3% donkey serum and 0.5% Triton X overnight at 4°C . They were then incubated with biotinylated donkey anti-mouse secondary diluted 1:500 overnight at

Table 1. Postmortem brain tissue

Donor brain	Sample	Age (yr)	Sex	PMI (h)	Brain region(s)	Lesion status
MS donor tissue						
MS1	1	67	F	2.5	Motor	GML
MS2	2	67	M	5.5	Parietal	GML
MS3	3	59	M	3.0	Motor	NAGM
MS4	4	76	M	8.0	Motor	NAGM
MS5	5	36	F	3.0	Parietal	GML
MS6	6	53	F	3.0	Parietal	NAGM
MS7	7	64	F	6.0	Motor	NAGM
MS8	8	64	F	6.0	Parietal	NAGM
	9	79	F	7.0	Motor	NAGM
MS9	10	79	F	7.0	Parietal	NAGM
	11	79	F	7.5	Motor	NAGM
MS10	12	79	F	7.5	Parietal	NAGM
	13	74	F	9.5	Motor	NAGM
MS11	14	74	F	9.5	Frontal	NAGM
	15	48	M	3.5	Parietal	NAGM
MS12	16	48	M	4.0	Parietal	GML
MS13	17	69	M	9.0	Motor	NAGM
	18	69	M	9.0	Parietal	NAGM
MS14	19	57	M	6.5	Motor	NAGM
	20	57	M	6.5	Parietal	NAGM
MS15	21	54	F	9.5	Motor	NAGM
	22	54	F	9.5	Parietal	NAGM
MS16	23	78	F	7.5	Motor	NAGM
	24	78	F	7.5	Parietal	NAGM
MS17	25	61	F	9.5	Motor	NAGM
	26	61	F	9.5	Parietal	NAGM
MS18	27	64	F	7.5	Motor	NAGM
	28	64	F	7.5	Parietal	NAGM
MS19	29	62	F	6.5	Motor	NAGM
	30	62	F	6.5	Parietal	NAGM
Control donor tissue						
C1	31	80	M	9.5	Motor	—
	32	80	M	9.5	Parietal	—
C2	33	91	F	10.0	Motor	—
	34	91	F	10.0	Parietal	—
C3	35	76	F	9.0	Motor	—
	36	76	F	9.0	Parietal	—
C4	37	58	M	9.0	Motor	—
	38	58	M	9.0	Frontal	—
C5	39	58	M	9.0	Parietal	—
	40	87	M	9.5	Motor	—
C6	41	87	M	9.5	Parietal	—
	42	35	F	9.5	Motor	—
C7	43	35	F	9.5	Parietal	—
	44	73	M	4.0	Motor	—
C8	45	49	F	5.0	Motor	—
C9	46	NA	M	9.0	Motor	—
C10	47	57	F	5.0	Motor	—
C11	48	51	M	8.0	Motor	—
C12	49	74	F	4.5	Parietal	—
C13	50	65	M	9.0	Parietal	—

NA, Not available; GML, subpial gray matter lesion.

4°C followed by incubation in Vector Elite ABC HRP solution (Vector Laboratories). PLP was visualized as a brown precipitate developed with the DAB reaction. Samples were coded and liquid chromatography tandem mass spectrometry (LC-MS/MS) was performed with 50–100 mg cortical gray matter from MS and control cortical tissue blocks to measure concentrations of methionine cycle metabolites. LC-MS/MS experiments were performed blinded as to the disease diagnosis of samples.

Measurement of NAA by high performance liquid chromatography (HPLC). Levels of NAA were measured in postmortem brain tissue by HPLC; 50 mg postmortem cortical gray matter adjacent to tissue analyzed for methionine metabolites by LC-MS/MS was analyzed. A Whatman Partisil 10 SAX anion-exchange column (4.6 mm × 250 mm) was

used in an Agilent 1100 Series HPLC Value System. The mobile phase consisted of 0.1 M KH₂PO₄ and 0.025 M KCl at pH 4.5. Retention data were collected at a flow rate of 1.5 ml/min, and the flow was monitored with an Agilent 1100 series UV detector at 214 nm. The retention time was determined with an NAA standard (Sigma). Peak areas were acquired with Agilent Chemstation software. NAA concentrations for MS and control brain tissue were determined in triplicate, and statistical significance of differences in NAA concentration between MS and control samples was determined with a two-tailed Student's *t* test, with *p* values ≤ 0.05 considered statistically significant.

Analysis of methionine metabolites by LC-MS/MS. Concentrations of methionine, SAM, SAH, cystathionine, choline, and betaine were analyzed by stable-isotope dilution liquid chromatography-electrospray ionization (ESI) tandem mass spectrometry (LC-ESI-MS/MS) from brain tissue as previously described (Inoue-Choi et al., 2013). Total homocysteine in brain tissue was measured by LC-ESI-MS/MS. Brain tissue was processed using a modified technique to extract protein bound homocysteine. Instead of precipitating the proteins with perchloric acid, the tissue was homogenized in 4× volume of buffer containing 5 mM dithiothreitol and 20 μM ²H₄-HCY and incubated on ice for 20 min. Homogenized samples were centrifuged at 14,000 rpm at 4°C for 10 min. Semiaqueous supernatant was transferred to a 10,000 MW cutoff filter unit and centrifuged at 14,000 rpm at 4°C for 25 min. The protein free filtrate was directly injected into the LC-MS/MS system. All metabolite analysis was performed on a Shimadzu Nexera LC System interfaced with a 5500QTRAP (ABSciex), and data were processed using Analyst software version 1.5.2. Changes in metabolite concentrations between MS and control samples were determined by a Student's *t* test, and correlations between metabolites were analyzed with Pearson's correlation analysis. *p* values were determined with a Student's *t* test, and changes were considered significant with *p* ≤ 0.05.

Cell culture. Human SH-SY5Y neuroblastoma cells were cultured in a 1:1 mixture of EMEM and F-12 medium (Sigma-Aldrich) with 10% FBS (MidSci) until 90% confluent. RNA and protein was isolated from these cells for RT-PCR and Western blotting experiments to confirm that they express betaine homocysteine methyltransferase (BHMT). Cells were then treated with either 400 μM of the nitric oxide (NO) donor sodium nitroprusside (SNP), 1 mM betaine, or both SNP and betaine to determine the effects of increased NO on histone H3 trimethylation (H3K4me3) levels and mitochondrial respiration and the ability of betaine to reverse these effects. To determine that SNP and betaine treatments were not detrimental to the cells, a trypan blue cell viability assay was performed. Briefly, 1 × 10⁶ SH-SY5Y cells were seeded into 12 well plates until 90% confluent and treated with either 400 μM SNP, 1 mM betaine, or both SNP and betaine overnight. The cells were detached and collected; 100 μl cell suspension was mixed 1:1 with 0.4% trypan blue solution and incubated at room temperature for 5 min. Cell numbers were counted under a microscope using a hemocytometer. To assess cell morphology, some cells were grown on coverslips and fixed after either SNP or betaine, or SNP/betaine treatments, and stained with antibodies to neurofilament (NF) (Millipore Bioscience Research Reagents) and BHMT (Thermosciences), and images were acquired with an Olympus FV1000 confocal microscope.

Western blotting. For BHMT Western blots, cytoplasmic fractions were isolated from a subset of MS and control postmortem brain samples, from mouse liver (for a positive control), and from SH-SY5Y cells; 10–40 μg protein was separated by electrophoresis in NuPAGE Bis-Tris polyacrylamide gels (Novex, Invitrogen), transferred to nitrocellulose, and incubated with antibodies to BHMT (monoclonal, Thermo Sciences) and GAPDH (Millipore Bioscience Research Reagents). For Western blots to quantitate mitochondrial electron transport chain complexes, mitochondrial fractions were isolated from a subset of MS and control tissue blocks containing adequate amounts of tissue for analysis. Mitochondrial fractions were blotted with mitochondrial antibodies to Complex I NADH dehydrogenase (ubiquinone) Fe-S protein 4 (NDUSF4) and Complex III ubiquinol-cytochrome *c* reductase core protein II (UQCRC2), both purchased from Mitosciences and aralar (Transduction Laboratories). Western blotting was also performed to determine relative levels of histone H3 lysine 9 dimethylation (H3K9me2) and

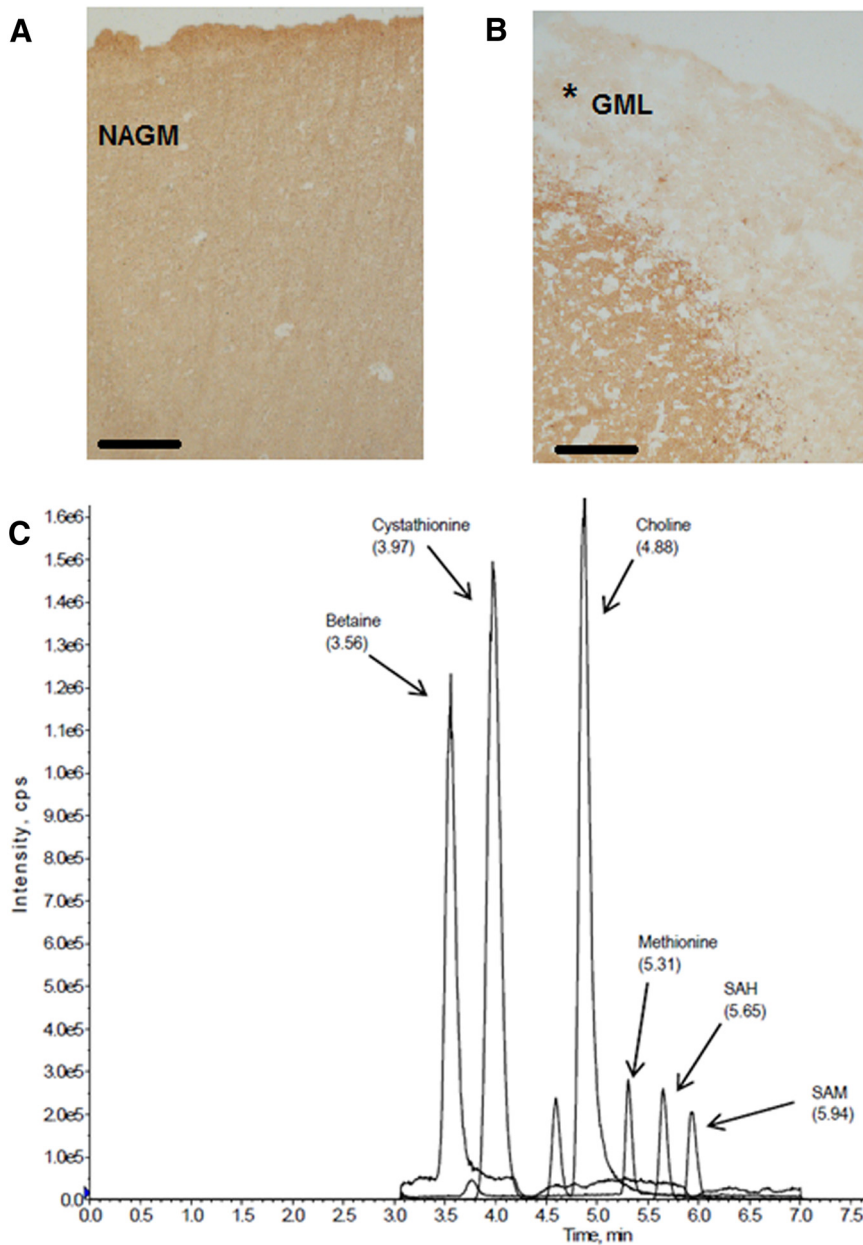


Figure 2. Analysis of methionine cycle metabolites in postmortem tissue by LC-MS/MS. Representative images acquired at $4\times$ magnification show normal appearing and lesioned gray matter. Immunohistochemistry was performed with a PLP antibody and the DAB reaction to assess lesion status of postmortem cortical tissue blocks analyzed by LC-MS/MS. **A**, Staining shows PLP immunoreactivity in NAGM. **B**, A subpial gray matter lesion (GML) in an MS cortical section is identified by the absence of DAB precipitate (*). Scale bar, $500\ \mu\text{m}$. **C**, Representative LC-MS/MS chromatogram from analysis of postmortem human brain tissue. Arrows indicate peaks for betaine, cystathionine, choline, methionine, SAH, and SAM.

H3K4me3 in MS and control gray matter and in SH-SY5Y cells treated with either SNP, betaine, or both SNP and betaine. For these experiments, nuclear protein was isolated and Western blotting with antibodies to H3K9me2, H3K4me3, and H3 (all from Abcam) was performed. For Western blotting with postmortem tissue, histones were isolated from a subset of MS and control samples (5 MS and 5 controls). Secondary antibodies conjugated to HRP were then added, and chemiluminescence was detected after the addition of luminol reagent (Santa Cruz Biotechnology). Quantitation of relative protein expression was performed by densitometry with ImageJ from at least three separate experiments. Levels of mitochondrial complex subunit proteins were normalized to the levels of the mitochondrial membrane protein aralar, and levels of H3K9me2 and H3K4me3 were normalized to total histone H3. Statistical

significance of changes in protein levels was determined by a two-tailed Student's *t* test with $p < 0.05$ considered significant.

qRT-PCR. Relative levels of mRNA for enzymes that catalyze one carbon metabolism reactions, including methionine synthase (*MTR*), methionine adenosyl transferase (*MAT*), SAH hydrolase (*AHCY*), *BHMT*, and cystathionine- β -synthase (*CBS*), were quantitated by qRT-PCR in mRNA isolated from gray matter from motor cortex from four control and five MS tissue blocks. qRT-PCR was performed with SYBR Green (Agilent Technologies) and gene-specific primers, which spanned an intron. Relative levels of mRNA expression in control and MS samples were determined by the $2^{-\Delta\Delta C_t}$ method after normalization to β -actin. Results are from three separate experiments. Statistical significance was determined with a two-tailed Student's *t* test with $p < 0.05$ considered significant.

For sequencing, *BHMT* mRNA was amplified by RT-PCR with the *BHMT* primers that spanned an intron from human postmortem cortex and from a human SH-SY5Y neuroblastoma cell line. Primers were synthesized to amplify the human *BHMT* mRNA sequence NM_001713 from 128 to 323. Primer sequences were as follows: *BHMT*, forward 5' AGGCCAAGAAGGGGATCCTA 3', and reverse 5' GTCTGCATGACGTTTGAGCC 3'. The RT-PCR band was gene cleaned and sequenced to confirm that *BHMT* mRNA was expressed in human postmortem cortex and in SH-SY5Y cells.

Immunohistochemistry. Blocks of frozen brain tissue were fixed in 4% PFA and cryoprotected with sucrose. Twenty to $30\ \mu\text{m}$ sections underwent immunohistochemical staining with antibodies to *BHMT* (monoclonal) and the NF-L antibody (both purchased from Thermo Sciences). Antigen retrieval was performed by placing sections in 100 mM sodium citrate buffer in an 800 W microwave oven for 2 min. Endogenous peroxidases were blocked in 0.3% H_2O_2 . Sections were blocked in 5% normal horse serum in PBS-Triton for 1 h and incubated overnight at 4°C in an antiserum to *BHMT* (1:250) in PBS + 5% horse serum + 0.3% Triton X followed by biotinylated anti-mouse secondary antibody (1:500) in PBS + 0.3% Triton X + 5% horse serum. Avidin biotin complex (1:500; Vector Laboratories) in PBS + 0.3% Triton X was added followed by a 10 min incubation in DAB chromogen. Sections were thoroughly rinsed in PBS and blocked in 5% horse serum for 1 h to be prepared for sequential immunohistochemistry stain with a second antibody. For the sequential stain, sections were incubated in NF-L antibody in 5% horse serum + 0.3% Triton X at 4°C overnight. On the second day, sections were rinsed in PBS, incubated for 1 h in secondary antibody (1:500) at room temperature, followed by 1 h incubation in avidin biotin complex (1:500; Vector Laboratories). A 20 min incubation in Alkaline Phosphate Blue (Vector Laboratories) chromogen visualized the reaction product. Sections were washed thoroughly in PBS, mounted on slides, cleared with ascending alcohol, and coverslipped with permount mounting medium.

Fluorescent imaging. Frozen tissue blocks from postmortem MS and control brains were fixed in 4% PFA for 24 h followed by washing in PBS ($2 \times 24\ \text{h}$). Tissue blocks were sliced using an oscillating tissue slicer

Table 2. Methionine metabolite concentrations in MS and control cortical gray matter tissue

	Homocysteine (nmol/g)	SAM (nmol/g)	SAH (nmol/g)	Methionine (nmol/g)	Cystathionine (nmol/g)	Betaine (nmol/g)	Choline (nmol/g)
MS (<i>n</i> = 30)	12.3 (±6.1)	12.5* (±3.7)	15.6 (±4.9)	88.7 (±44.8)	525* (±469)	47.8* (±30.8)	232 (±115)
Control (<i>n</i> = 20)	13.2 (±7.0)	15.5 (±6.4) <i>p</i> = 0.04	17.0 (±4.0)	99.9 (±59.3)	1389 (±1054) <i>p</i> = 0.0002	85.5 (±48.0) <i>p</i> = 0.001	247 (±159)

The asterisks denote significance between MS and control concentrations (*p* < 0.05).

Table 3. Methionine metabolite concentrations in motor and parietal cortex

	Homocysteine (nmol/g)	SAM (nmol/g)	SAH (nmol/g)	Methionine (nmol/g)	Cystathionine (nmol/g)	Betaine (nmol/g)	Choline (nmol/g)
Motor cortex							
MS (<i>n</i> = 10)	14.1 (±5.5)	11.9 (±3.6)	14.8 (±6.1)	86.6 (±34.0)	442* (±427)	45.9 (±28.4)	241 (±129)
Control (<i>n</i> = 6)	17.5 (±5.0)	13.5 (±6.5)	15.5 (±3.1)	74.3 (±33.7)	1495 (±1154) (<i>p</i> = 0.02)	79.4 (±54.5)	332 (±192)
Parietal cortex							
MS (<i>n</i> = 10)	11.0 (±2.8)	12.9 (±4.7)	14.9 (±5.5)	100.5 (±65.6)	445* (±473)	50.6* (±37.2)	215 (±139)
Control (<i>n</i> = 6)	17.3 (±6.0)	13.5 (±5.0)	15.5 (±2.3)	87.8 (±38.1)	1453 (±1149) (<i>p</i> = 0.03)	104.0 (±51.2) <i>p</i> = 0.03	273 (±137)

The asterisks denote significance between MS and control concentrations (*p* < 0.05).

(EMS) at 30 μ m, and free-floating sections were incubated in the appropriate antibody. To visualize BHMT immunoreactivity, tissue sections were incubated in rabbit anti-BHMT (1:250; polyclonal) (Thermosciences) and rabbit anti-NeuN (1:200) (Millipore Bioscience Research Reagents). To measure H3K4me3 fluorescence, sections were incubated in rabbit anti-H3K4me3 (1:200) (Abcam) and mouse anti-NeuN antibodies. All incubations were done in PBS, 0.5% Triton X-100, and 3% donkey serum overnight at 4°C. Tissue sections were then incubated in donkey anti-rabbit Alexa-488 (1:400) and donkey anti-mouse Alexa-555 (1:400) for 3 h at 4°C. Both secondary antibodies were purchased from Invitrogen. Following 3 \times 10 min washes in PBS, sections were incubated in 50 mM ammonium acetate, 10 mM cupric sulfate for 30 min to quench lipofuscin autofluorescence. Sections were washed and mounted with Vectashield mounting medium containing DAPI to label nuclei. Images were acquired with an Olympus Fv1000 confocal microscope equipped with five laser lines (HeCd 442 nm, Ar 488 and 514 nm, HeNe 543 nm and HeNe 633 nm). Image stacks were *z*-projected with ImageJ (National Institutes of Health) and channels merged to show colocalized signals. Relative H3K4me3 fluorescence was compared in MS and control tissue blocks (C1, C2, MS5, and MS18). Image stacks were captured sequentially for each channel to prevent bleed through and spanned the sections. An image mask was created using the NeuN channel as a guide to include the entire nucleus. The thresholded image mask was then used to clip the H3K4me3 channel, and the pixels within the unclipped region were summed. This technique measures the amount of H3K4me3 fluorescence from within individual NeuN-stained nuclei. Mean density of H3K4me3 immunofluorescence was obtained from the average intensity from at least 50 NeuN-positive neuronal nuclei from two control and two MS samples.

Respirometry. To determine whether the BHMT–betaine pathway could support respiration after treatment with SNP, an XF24 Extracellular Analyzer (Seahorse Bioscience) was used to measure the oxygen consumption rate (OCR) and spare respiratory capacity in mitochondria isolated from SHSY-5Y cells treated with either 400 μ M SNP or 1 mM betaine, or both 400 μ M SNP + 1 mM betaine. Mitochondria were isolated by homogenizing cells in MSHE + BSA (70 mM sucrose, 210 mM mannitol, 5 mM HEPES, 1 mM EGTA, and 0.5% BSA) with a glass homogenizer at 4°C. The cell suspension was then centrifuged at 1000 \times *g* for 10 min at 4°C. The supernatant was centrifuged again at 8000 \times *g* for 10 min at 4°C, the pellet was resuspended, and total protein (mg/ml) was determined using Bradford Assay reagent (Bio-Rad). For the assay, mitochondria were diluted 10 times in cold 1 \times MAS + substrate (70 mM sucrose, 220 mM mannitol, 2 mM HEPES, 10 mM KH₂PO₄, 5 mM MgCl₂, 1 mM EGTA, and 0.2% BSA + 10 mM succinate and 2 μ M rotenone), and then plated on the XF assay plate in equal concentration (5 μ g). This assay measures electron transport activity through Complexes II–IV; 50 μ l of mitochondrial suspension was delivered to each well (except for background correction wells). The XF cell culture microplate was centrifuged at 2000 \times *g* for 20 min at 4°C to adhere the mitochondria. The plate was then transferred to the XF analyzer, and the experiment was initiated. Injection of ADP (4 mM final), oligomycin (2.5 μ g/ml final), FCCP (4 μ M

final), and antimycin A (4 μ M final) to inhibit Complex III was added sequentially, and the OCR was monitored over time. The OCR was calculated in pmol/min. Basal respiration was monitored initially. Maximal respiratory capacity was measured after addition of oligomycin to block ATP synthase and the uncoupler FCCP, which eliminates the proton gradient (and respiratory control exerted by the proton gradient) across the mitochondrial inner membrane and stimulates maximal oxygen consumption. Spare respiratory capacity was calculated by subtracting basal respiration, including nonmitochondrial oxygen consumption measured after addition of antimycin A, from the maximal respiration. Average changes in basal, maximal, and spare respiratory capacity were determined in triplicate. Statistical significance was determined by a two-tailed Student's *t* test, with *p* < 0.05 considered significant.

Chromatin immunoprecipitation (ChIP)-seq. To identify genes regulated by betaine in SH-SY5Y neuroblastoma cells, chromatin immunoprecipitation followed by Illumina-based sequencing (ChIP-seq) was performed with an antibody to H3K4me3 and chromatin isolated from control SH-SY5Y cells and cells treated with 1 mM betaine overnight. For ChIP, cells were fixed with 37% formaldehyde solution for 10 min followed by washing with PBS. The fixation was stopped by adding 1 \times glycine stop-fix solution for 5 min. The cells were lysed to release the nuclei and centrifuged at 2400 \times *g* at 4°C for 10 min to pellet the nuclei. Chromatin was resuspended in RIPA buffer containing protease inhibitors (Sigma) and was sheared by sonication with a focused ultrasonicator (Covaris) for 8 min to obtain chromatin fragments 300–400 bp in length. Fragment size was confirmed on an Agilent 2100 Bioanalyzer (Agilent Technologies); 10 μ l of sheared sample (input DNA) was stored at –20°C to be used as a control. ChIP was performed with the ChIP-IT Express kit provided by Active Motif. ChIP reactions were set up by sequential addition of 25 μ l protein G magnetic beads, 20 μ l of ChIP buffer, 50 μ g of sheared chromatin, 2 μ l of protease inhibitor mixture, distilled water to makeup the final volume 200 μ l, and 4 μ g of H3K4me3 antibody (Abcam) followed by incubation on an end-to-end rotor at 4°C overnight. Beads were separated on a magnetic stand, washed, and then resuspended in 50 μ l of elution buffer. Chromatin was cleaned up by treatment with proteinase K followed by phenol-chloroform extraction and EtOH precipitation.

DNA sequences enriched in ChIP DNA from betaine-treated cells compared with input DNA and control ChIP DNA were identified by high throughput sequencing. Input DNA and ChIP DNA from control and betaine-treated cells were quantified using the Qubit dsDNA HS Assay Kit (Invitrogen). Sequencing libraries were prepared from 10 ng of DNA using the TruSeq ChIP Sample Preparation Kit (Illumina) following the manufacturer's recommendation. Libraries were purified and size selected using a 2% low-melting agarose gel (Invitrogen) by cutting a band of 250–300 bp on a 2% agarose gel, resulting in a 150–200 bp insert size. The libraries were enriched using an 18 cycle PCR program. Enriched libraries were quantified by qPCR using the KAPA Library Quantification Kits (KAPA Biosystems). The Agilent Bioanalyzer 2100 DNA High Sensitivity kit was used to assess the library quality and size distribution. The libraries were sequenced on a HiSeq2500 (Illumina) in the Cleveland Clinic Lerner Research Institute Genomics Core using a 50 bp

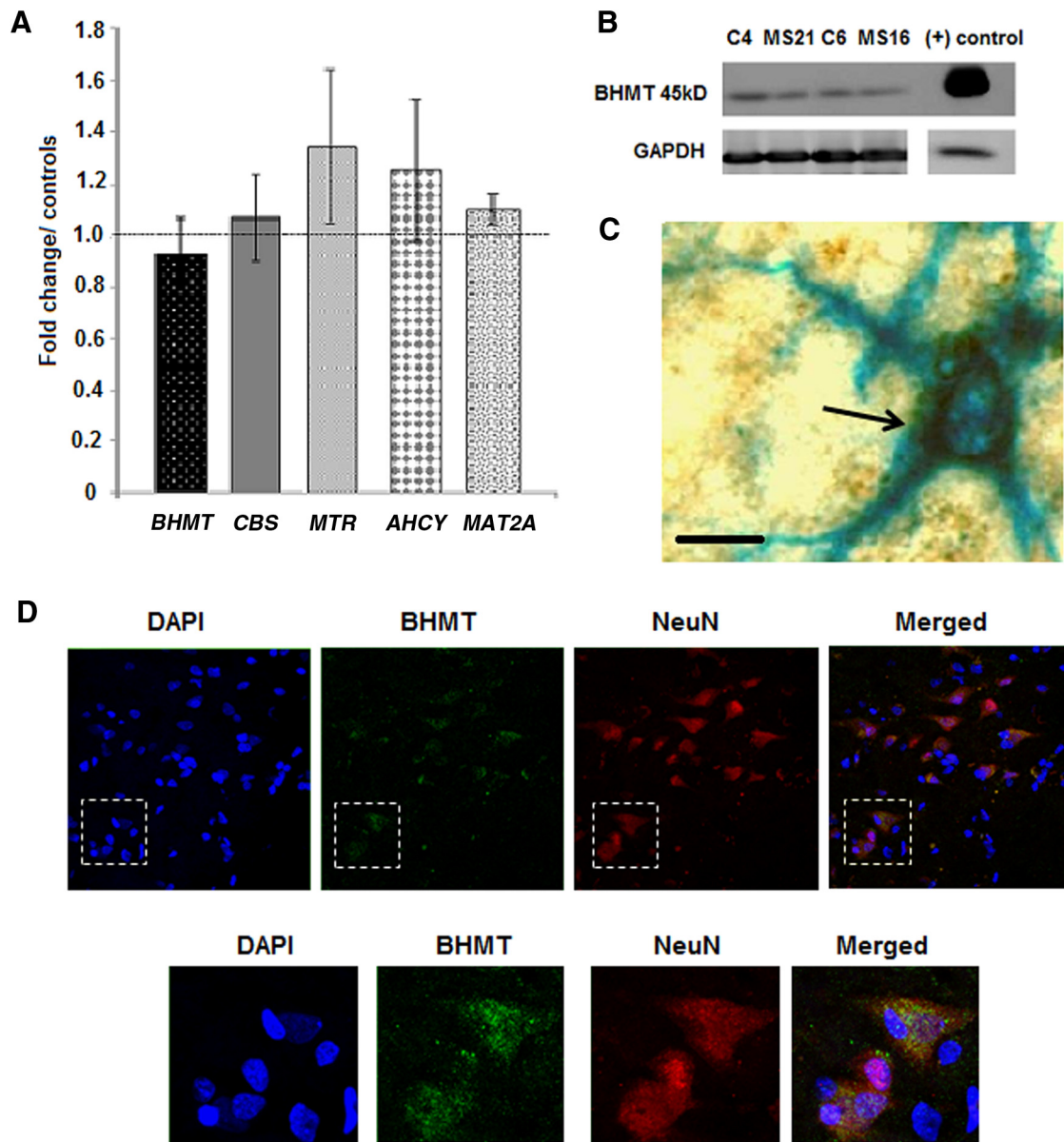


Figure 3. BHMT is expressed in neurons in the CNS. **A**, qRT-PCR for one carbon metabolism enzymes *BHMT*, *CBS*, *MTR*, *AHCY*, and *MAT2A* shows that enzyme expression is not changed in MS samples compared with controls. Average expression levels are shown for MS samples as a percentage of control levels, which were set at 100% (shown by dotted line). Error bars indicate SEM. **B**, Western blotting for BHMT expression in postmortem MS, and control brain tissue shows that the BHMT protein is present in low levels in the CNS. Positive control sample is protein isolated from mouse liver. GAPDH band for the positive control is from a longer exposure. **C**, Immunohistochemistry shows colocalization of NF (blue alkaline phosphatase staining) and BHMT immunoreactivity (brown DAB precipitate) denoted by arrow on cortical tissue sections. Original magnification 60 \times . Scale bar, 20 μ m. **D**, Top, Representative confocal images acquired at 60 \times showing immunofluorescent staining for BHMT (green) and NeuN (red) in a postmortem cortical tissue section (MS6). Nuclei are stained with DAPI (blue). Area outlined in the white box was enlarged and is shown (bottom). Green fluorescence indicating BHMT immunoreactivity can be seen colocalized in neurons also stained with NeuN.

single end reads. Fastq sequences were aligned and analyzed with Strand NGS 2.5 software (Avadis) with default settings, including an alignment quality against reference of 90%. Peak detection and regions of H3K4me3 enrichment over input DNA and with increased reads as a result of betaine treatment were detected with the Model-based Analysis of Chip-Seq algorithm with a Q score (FDR) cutoff of 0.001 (Zhang et al., 2008). H3K4me3-enriched peaks were mapped to human RefSeq transcripts (NCBI hg19) and annotated for genes within 20 kb of transcription start sites (TSSs) or within genes or introns. Functional categories of genes enriched by ChIP-seq were assigned with PANTHER (<http://pantherdb.org/>). Gene expression changes for a subset of genes enriched by ChIP-seq were confirmed by qRT-PCR with gene-specific primers and Brilliant III Ultra-Fast SYBR Green (Agilent Technologies). qRT-PCR was performed with RNA isolated from control SH-SY5Y cells and cells treated with SNP, betaine, or SNP/betaine. Fold changes in gene expres-

sion were calculated with the $2^{-\Delta\Delta Ct}$ method after normalization to actin. Data are the average fold change from at least three experiments. Statistical significance was determined with a two-tailed Student's *t* test with $p < 0.05$ considered significant.

Results

Methionine metabolite concentrations were measured in 50 motor, frontal, and parietal cortex tissue blocks from 32 MS and control brains. Donor and tissue characteristics, including age and sex of the donors and PMI, brain region, and lesion status of tissue analyzed, are described in Table 1. MS and control tissue blocks were matched for age, sex, and PMI as closely as possible. The average age of donors did not differ significantly between MS (63 \pm 12 years) and control donors (66 \pm 17 years). We have

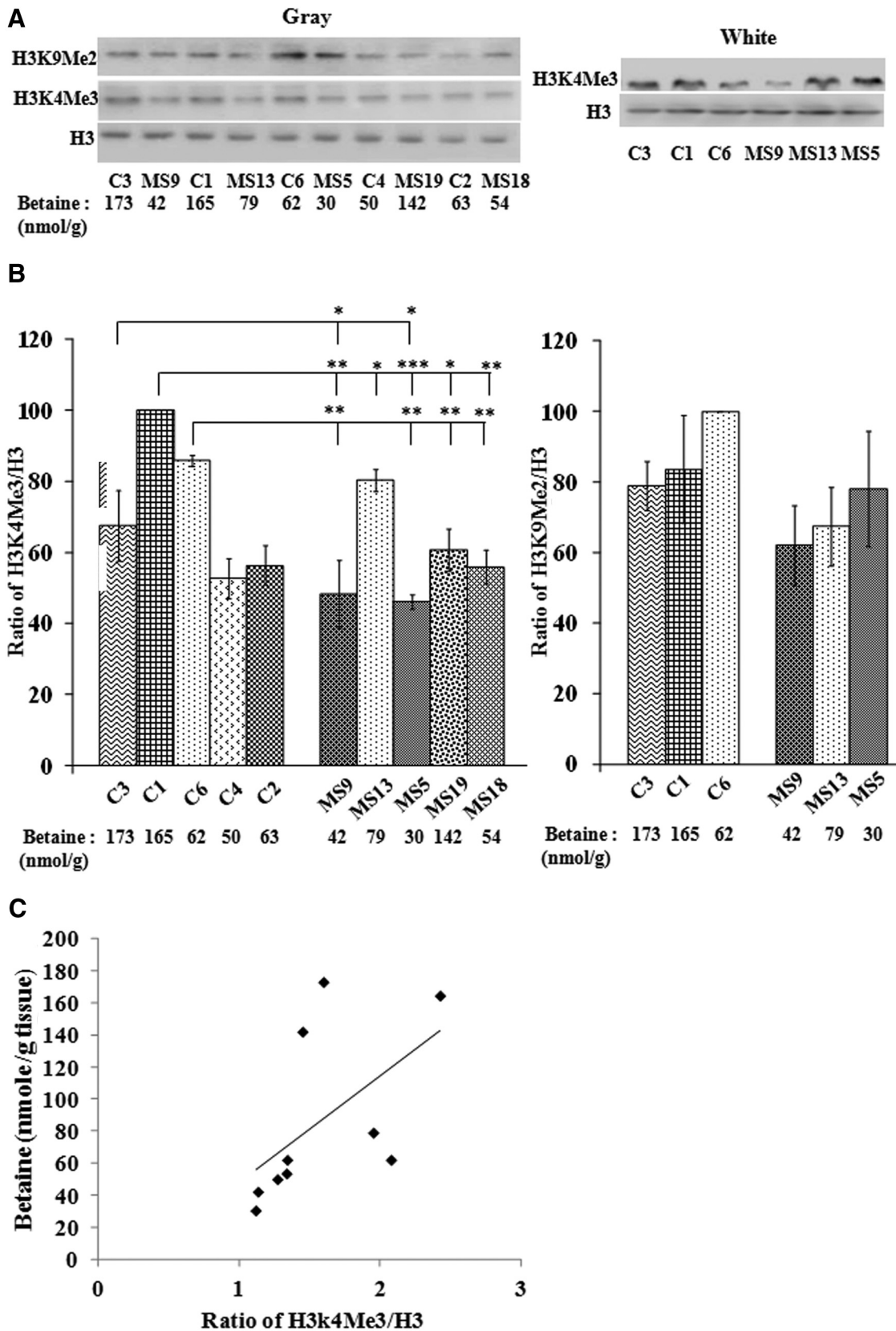


Figure 4. Levels of H3K4me3 are decreased in MS cortical gray matter and are correlated with levels of betaine. **A**, Representative Western blots for H3K9me2, H3K4me3, and histone H3 from histones isolated from MS and control gray and white matter cortical samples. **B**, Densitometry performed from three separate experiments shows that H3K4me3 is decreased in MS gray matter samples compared with controls, whereas H3K9me2 is not significantly changed. Relative H3K4me3/H3 and H3K9me2/H3 levels are expressed as a percentage of control with the highest control set at 100%. Betaine concentrations are shown for each MS and control sample. **C**, Pearson’s correlation analysis was performed and shows that relative levels of H3K4me3 are correlated to betaine concentrations measured by LC-MS/MS in the same tissue blocks. Pearson’s correlation coefficient: $r = 0.55, p = 0.049$. Error bars indicate SEM. * $p < 0.05$. ** $p < 0.01$. *** $p < 0.001$.

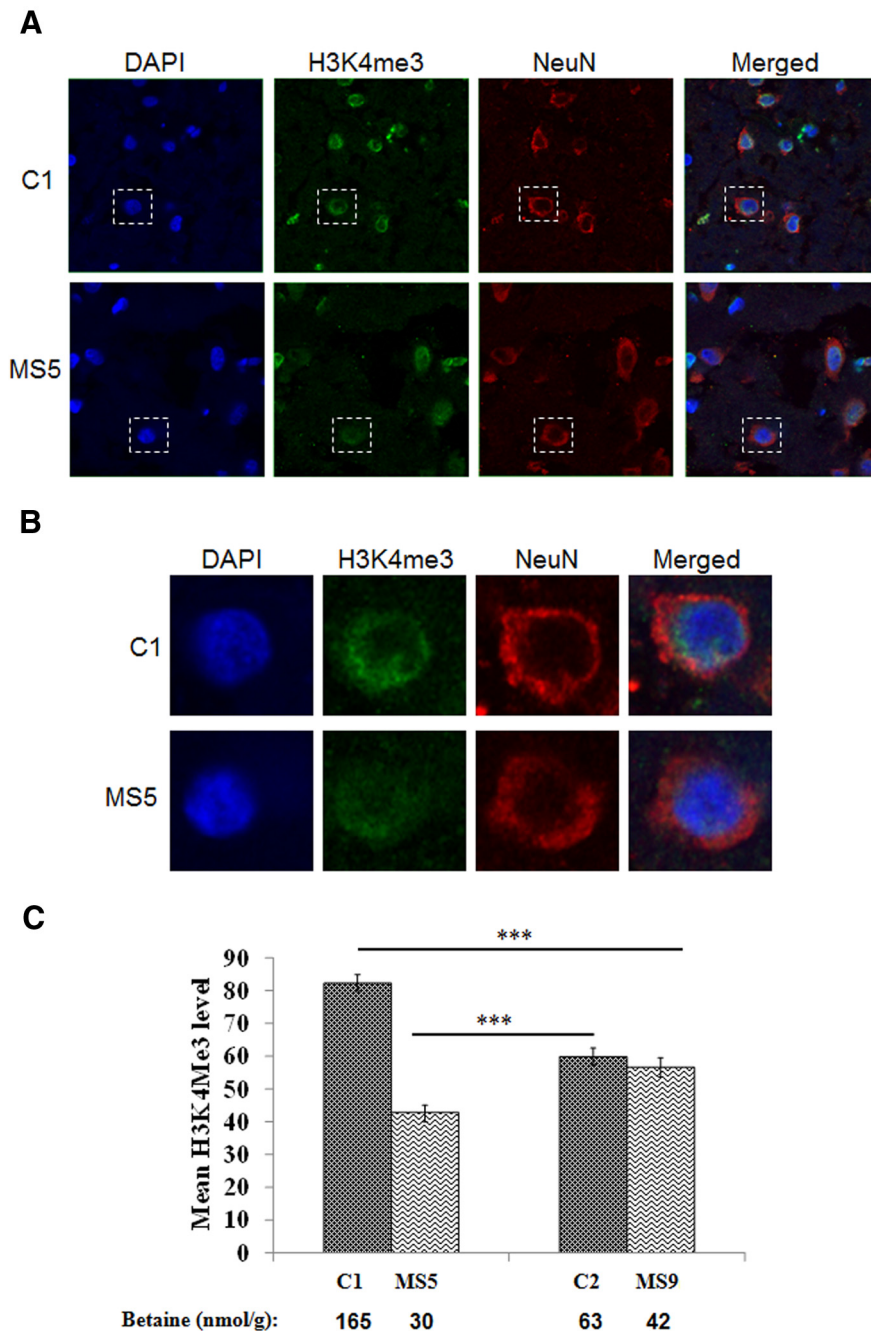


Figure 5. H3K4me3 is decreased in neurons in MS cortex. **A**, Representative confocal images of DAPI (blue), H3K4me3 (green), and NeuN (red) immunofluorescent staining in MS and control cortical tissue sections. **B**, Cells outlined in **A** were enlarged to show individual neuronal nuclei. **C**, Bar diagram represents mean density of H3K4me3 fluorescence measured in NeuN-positive nuclei in MS and control tissue sections. Error bars indicate SEM. $***p \leq 0.001$ (two-tailed paired *t* test).

found that SAM degrades at room temperature after ~ 15 h (data not shown), so all tissue PMIs were ≤ 10 h. The average PMI for MS samples was 6.2 ± 2.4 h and for controls was 7.7 ± 2.2 h. Representative PLP immunohistochemistry to assess lesion status of tissue blocks analyzed is shown in Figure 2. Of the MS samples analyzed, four contained subpial gray matter lesions of the type shown in Figure 2B, and all others were normal appearing gray matter (NAGM). Representative LC-MS/MS chromatograms for methylation metabolites SAM, SAH, methionine, cystathionine, betaine, and choline obtained from postmortem brain tissue are shown in Figure 2C. Quantitation for methylation metabolites indicates that average concentrations of cysta-

thionine, SAM, and betaine are significantly decreased in MS samples as shown in Table 2. The methyl donors SAM and betaine were decreased in MS samples by 19% ($p = 0.04$) and 44% ($p = 0.001$), respectively. Concentrations of cystathionine, the first step for the transsulfuration pathway that generates the redox regulator GSH, were decreased by 62% ($p = 0.0002$) in MS. Homocysteine levels were not significantly changed in MS samples overall but were negatively correlated with SAM concentrations ($r = -0.30$, $p = 0.04$). The average concentration of the methionine metabolites in MS tissue blocks containing subpial gray matter lesions was similar to levels observed in NAGM for MS samples (data not shown). We also compared methionine metabolite concentrations between brain regions. Analyzing both parietal and motor cortex tissue blocks from the same 10 MS and 6 control brains, we observed significant changes in cystathionine and betaine concentrations in MS as shown in Table 3. Cystathionine was decreased by 70% ($p = 0.02$) in MS motor cortex. Both cystathionine and betaine concentrations were decreased in parietal cortex in MS samples by 69% ($p = 0.03$) and 51% ($p = 0.03$), respectively.

We also quantitated the mRNA expression of enzymes involved in methionine metabolism (Fig. 1), including *MAT2A*, *AHCY*, *MTR*, *CBS*, and *BHMT*, by qRT-PCR. These data show that mRNA expression was not altered for any of these enzymes in MS samples compared with controls as shown in Figure 3A. However, of particular interest, we detected *BHMT* mRNA in our samples, indicating that this enzyme may be expressed in the CNS. The presence of *BHMT* mRNA was confirmed by sequencing of the RT-PCR product (data not shown). *BHMT* catalyzes the conversion of homocysteine to methionine with betaine as the methyl donor as shown in Figure 1, and this reaction has previously been thought to occur only during embryonic development and in liver and kidney in the adult in humans (Lever and Slow, 2010). To confirm the presence of *BHMT* protein in brain tissue, we performed Western blotting on protein isolated from MS and control cortex and observed *BHMT* immunoreactivity as shown in Figure 3B. Localization of *BHMT* expression in the CNS was confirmed by immunohistochemistry on postmortem tissue sections. As shown in Figure 3C, cytoplasmic *BHMT* staining (brown DAB precipitate) was present in neurons coexpressing the neuronal specific NF light chain protein (blue alkaline phosphatase reaction precipitate). *BHMT* appears as cytoplasmic staining around the nucleus and was not observed along axons. We also performed confocal microscopy

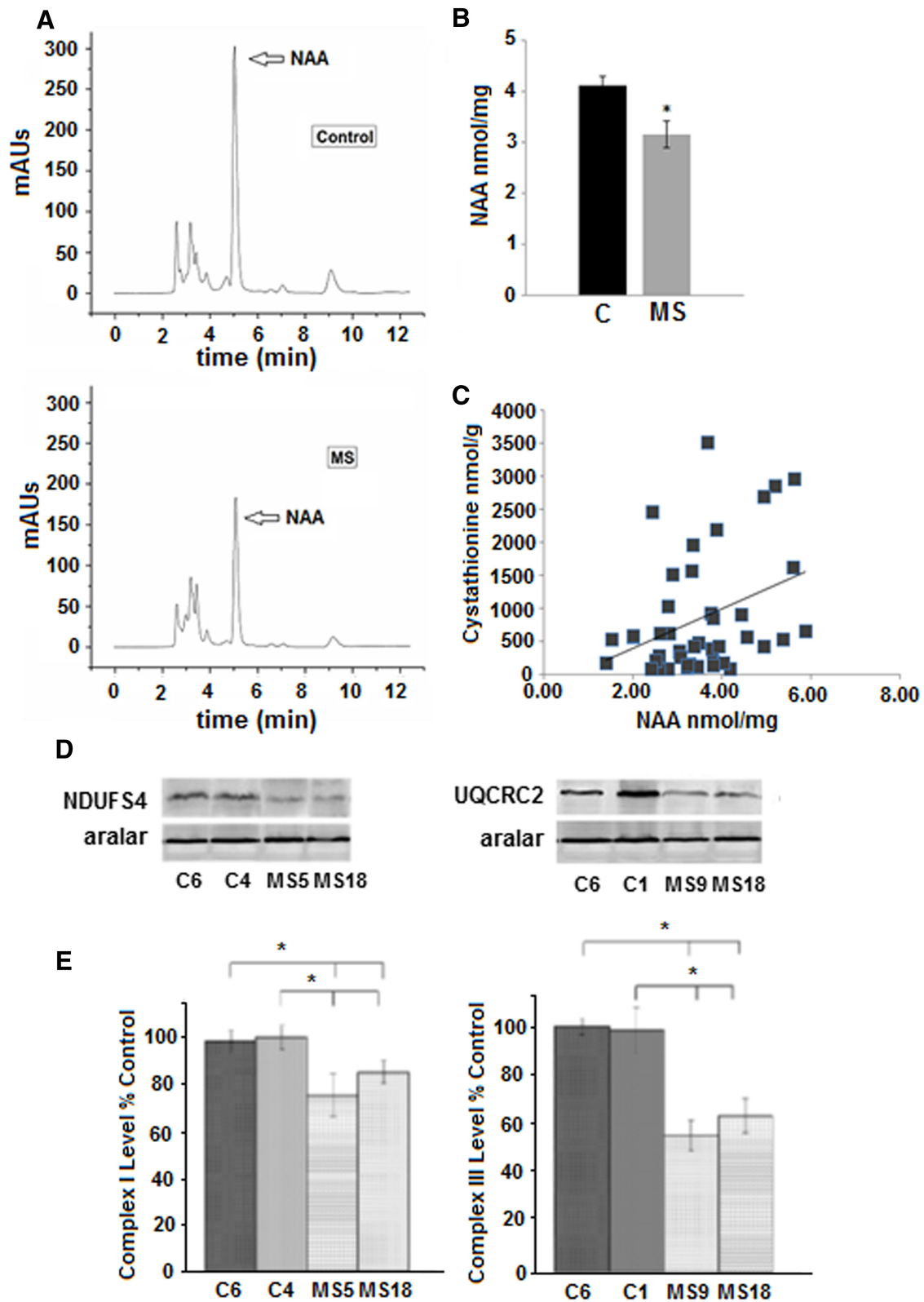


Figure 6. Markers of mitochondrial respiration are decreased in MS samples. NAA is decreased in MS and correlated with cystathionine concentrations. **A**, Representative HPLC chromatograms for quantification of NAA from an MS and control brain tissue sample. The NAA peak eluted at 5.1 min. **B**, Quantitation of average NAA concentrations in MS ($n = 27$) and control ($n = 17$) samples adjacent to tissue analyzed for methionine metabolites by LC-MS/MS show that NAA is decreased by 24% in MS samples analyzed in this study. Error bars indicate SEM. $*p < 0.05$. **C**, Pearson's correlation analysis was performed and shows that NAA levels are positively correlated with cystathionine concentrations ($r = 0.35, p = 0.02$). Mitochondrial electron transport chain subunits were also found to be decreased in MS gray matter samples. **D**, Representative Western blots performed with mitochondrial fractions isolated from MS and control gray matter samples probed for the mitochondrial electron transport chain subunits, Complex I NDUF54, Complex III UQCRC2, and the mitochondrial membrane protein aralar. **E**, Levels of mitochondrial electron transport chain subunit proteins in control and MS samples were determined by densitometry. Relative levels of NDUF54 and UQCRC2 proteins are normalized to the mitochondrial membrane protein aralar and are shown as percentage of control. Error bars indicate SEM. $*p < 0.05$.

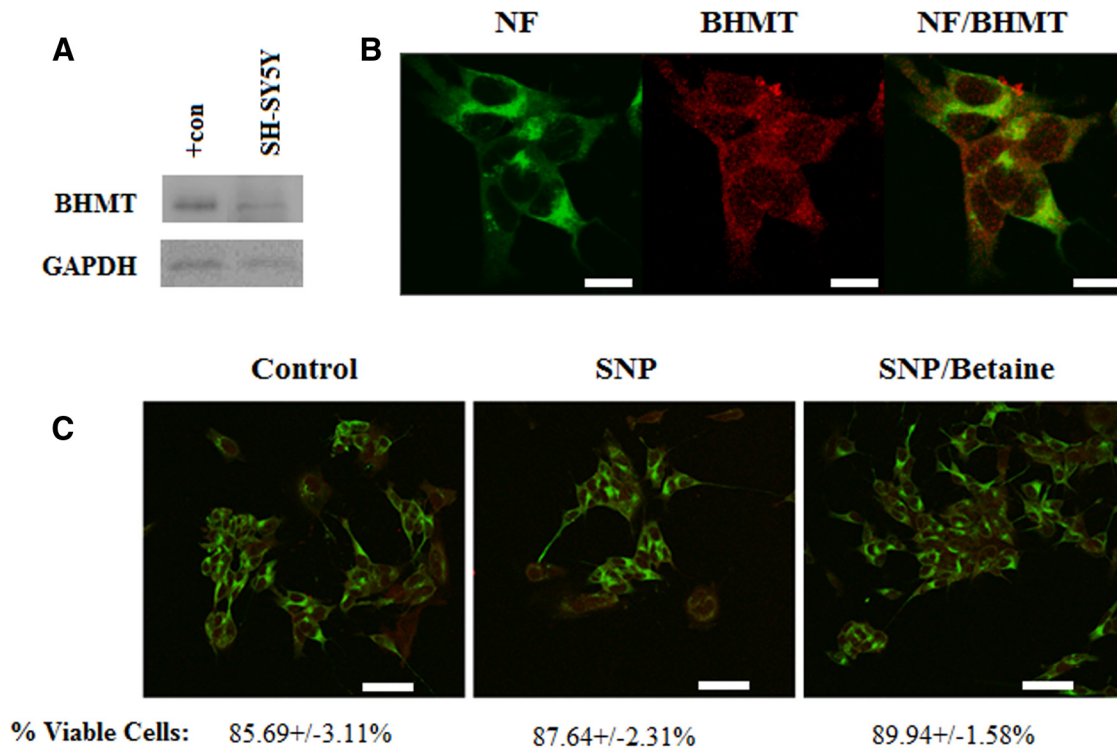


Figure 7. BHMT is expressed in SH-SY5Y neuroblastoma cells. **A**, Representative Western blot showing that the 45 kDa BHMT protein is expressed in SH-SY5Y cells. The positive control for BHMT expression is protein isolated from mouse liver. **B**, Immunofluorescent staining with antibodies to NF shown in green fluorescence and BHMT (red fluorescence) show BHMT immunoreactivity in SH-SY5Y cells. Scale bars, 15 μ m. Confocal images were acquired at 100 \times . **C**, To assess cell morphology after SNP and betaine treatments, control SH-SY5Y cells, and cells treated with 400 μ M SNP or 400 μ M SNP and 1 mM betaine were immunostained for NF (green fluorescence) and BHMT (red fluorescence). Scale bars, 50 μ m. Confocal images were taken at 40 \times . Trypan blue cell viability assay data are shown as percentage viable cells \pm SD beneath the images.

to localize BHMT expression in postmortem human tissue sections as shown in Figure 3D. BHMT expression (green fluorescence) can be seen in cells expressing the neuronal marker NeuN (red fluorescence). These experiments confirm cytoplasmic BHMT expression in neurons.

To determine whether there are functional consequences of decreased levels of the methyl donors SAM and/or betaine on methylation of substrates, we examined histone H3 methylation patterns in MS and control cortical samples. We analyzed H3K9me2 and H3K4me3 by Western blotting and immunofluorescent staining. H3K9me2 is repressive and is found in heterochromatin. Decreased H3K9me2 has been shown to mediate chromatin relaxation, resulting in aberrant gene expression and neurodegeneration in *Drosophila* and mouse models of Alzheimer's disease (AD) and in postmortem AD brain tissue (Frost et al., 2014). The H3K4me3 modification is present in active chromatin (Sandstrom et al., 2014) and has important implications for transcriptional activation of genes involved in mitochondrial respiration, which have been previously demonstrated to be altered in MS cortex. Western blotting was performed with histones isolated from MS and control cortex and antibodies to H3K4me3 and H3K9me2 in a subset of MS and control samples. Representative Western blots and quantitation for H3K4me3 and H3K9me2 are shown in Figure 4A,B. These data show that H3K4me3 was decreased in MS gray matter, but not in white matter (quantitation not shown). Pearson's correlation analysis revealed that H3K4me3 levels measured by Western blotting were correlated with levels of betaine ($r = 0.55$, $p = 0.049$) measured in adjacent tissue from the same tissue blocks as shown in Figure 4C. The levels of H3K9me2 showed greater variability between samples than H3K4me3 and were not found to be sig-

nificantly changed between MS and control samples (Fig. 4B). Decreased levels of H3K4me3 in gray but not white matter cortical tissue suggest that this change is occurring in the nuclei of a cell type enriched in gray matter. Neuronal cell bodies and nuclei are enriched in gray matter, but many other cell types, including oligodendrocytes, astrocytes, and microglia, are also present. To determine whether H3K4me3 was decreased specifically in neurons, the fluorescence intensity of H3K4me3 staining was measured in the nuclei of at least 50 NeuN-positive cells in a subset of samples (C1, C2, MS5, and MS18) exhibiting varying levels of betaine. Representative confocal images showing nuclear H3K4me3 expression in an MS and a control sample are shown in Figure 5A,B. Quantitation shows that H3K4me3 staining was correlated with betaine levels measured by LC-MS/MS in adjacent tissue and was decreased in neuronal nuclei in MS samples exhibiting low betaine (Fig. 5C).

The H3K4me3 histone mark has been shown to be involved in transcriptional activation of mitochondrial electron transport chain genes (M. Soloveychik and M. Meneghini, personal communication). To determine whether decreased levels of H3K4me3 could be mediating changes in electron transport chain gene expression and neuronal respiration in MS, we measured respiratory status in the postmortem cortical samples by quantitating levels of NAA. Levels of NAA have been shown to be related to neuronal mitochondrial electron transport chain activity (Li et al., 2013) and provide a measurement of axonal integrity and neuronal mitochondrial activity within tissue. Representative HPLC chromatograms for NAA obtained from an MS and control sample are shown in Figure 6A. HPLC analysis for NAA concentration was performed in MS and control cortical samples with sufficient tissue (27 MS and 17 control samples). These data

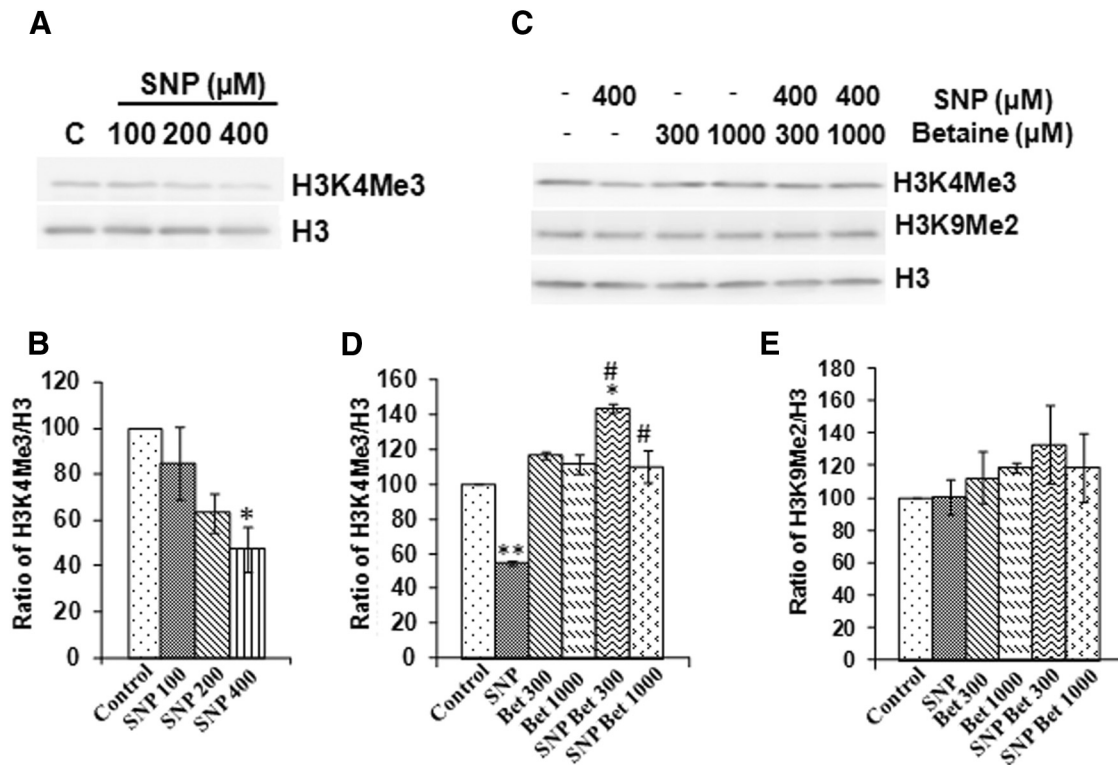


Figure 8. Betaine rescues H3K4me3 levels and mitochondrial respiration in SH-SY5Y cells after treatment with the NO donor SNP. **A**, Western blotting with nuclear protein isolated from SH-SY5Y cells treated with 100, 200, or 400 μM SNP and an antibody to H3K4me3 shows reduced levels of H3K4me3 with 400 μM SNP treatment. **B**, Bar graphs represent quantitation of H3K4me3 levels normalized to histone H3 levels in control and SNP-treated cells. **C**, Representative Western blots for H3K4me3 and H3K9me2 with nuclear protein isolated from SH-SY5Y cells treated with 400 μM SNP, 300 μM betaine, 1000 μM betaine, or both SNP and betaine. **D**, Quantitation of H3K4me3 was performed by densitometry from control SH-SY5Y cells and cells treated with SNP, betaine (Bet), and SNP/betaine. **E**, H3K9me2 levels are not changed in SH-SY5Y cell nuclear extracts after SNP or betaine treatment. Concentrations of SNP and betaine are in μM . H3K4me3 and H3K9me2 levels were normalized to H3. * $p < 0.05$ versus control. ** $p < 0.01$ versus control. # $p < 0.05$ versus SNP-treated cells.

show that mean NAA concentrations are decreased in MS (Fig. 6B), suggesting decreased neuronal energetic capacity in MS samples. Decreased NAA levels were found to be correlated with the concentration of the methionine metabolite cystathionine measured by LC-MS/MS in adjacent tissue with Pearson's correlation analysis ($r = 0.35$, $p = 0.02$) as shown in Figure 6C. We also analyzed mitochondrial electron transport chain subunit protein levels in a subset of samples with adequate amounts of tissue for analysis by Western blotting. Mitochondrial fractions isolated from MS and control cortical gray matter samples were probed with antibodies to the electron transport chain subunits previously found to be decreased in MS including the Complex I NDUSF4 protein and the Complex III UQCRC2 subunit. Representative Western blots and quantitation are shown in Figure 6D,E. These data show that, in addition to decreased NAA, electron transport chain complex subunits are also decreased in MS samples compared with controls.

We then performed Western blotting, immunohistochemistry, and RT-PCR followed by sequencing to determine whether BHMT mRNA and protein are expressed in the human SH-SY5Y neuroblastoma cell line. RT-PCR followed by sequencing confirmed that *BHMT* mRNA is expressed in SH-SY5Y cells (data not shown). We found that BHMT protein was also present in these cells (Fig. 7), which then provided a model for us to investigate the role of betaine on H3K4me3 levels and mitochondrial respiration under the type of inflammatory conditions that exist in MS. We first treated human SH-SY5Y neuroblastoma cells with the NO donor SNP (400 μM) and also with betaine (1 mM) and performed immu-

nohistochemistry with antibodies to NF and BHMT to be sure there were no gross changes in cell morphology (Fig. 7C). We also tested cell viability with the trypan blue assay, and the percentage of viable cells \pm SD are also shown in Figure 7C. These data show that neither SNP nor betaine treatment caused a reduction in the numbers of viable SH-SY5Y cells. The percentage of viable cells were $85.69 \pm 3.11\%$ for control cells, $87.64 \pm 2.31\%$ for SNP treated cells, $89.98 \pm 2.18\%$ for betaine-treated cells (not shown in Fig. 7), and $89.94 \pm 1.58\%$ for SNP/betaine-treated cells.

We then treated SH-SY5Y cells with 100 μM –400 μM SNP and measured H3K4me3 levels by Western blot to determine whether increased NO could mediate changes to H3K4me3 similar to what we observed in the MS brain. We found that 400 μM SNP decreased H3K4me3 in SH-SY5Y cells by $\sim 50\%$ compared with controls (Fig. 8A,B). We then supplemented cell culture media with betaine to test the efficacy of betaine on reversing SNP-mediated decreases in H3K4me3 (Fig. 8C,D). We found that neither 300 μM nor 1 mM betaine alone significantly increased H3K4me3, but betaine did increase H3K4me3 levels in SNP-treated cells even above controls. We also tested the effect of SNP and betaine on the levels of the repressive H3K9me2 methyl mark and found that this modification was not significantly altered by SNP or betaine treatment (Fig. 8E). This may reflect the fact that H3K4me3 is a dynamic methyl mark present in transcriptionally active and accessible chromatin, whereas H3K9me2 is localized in transcriptionally silent heterochromatin (Börsch-Haubold et al., 2014).

To determine whether changes in betaine concentration and H3K4me3 levels can impact mitochondrial respiration, we mea-

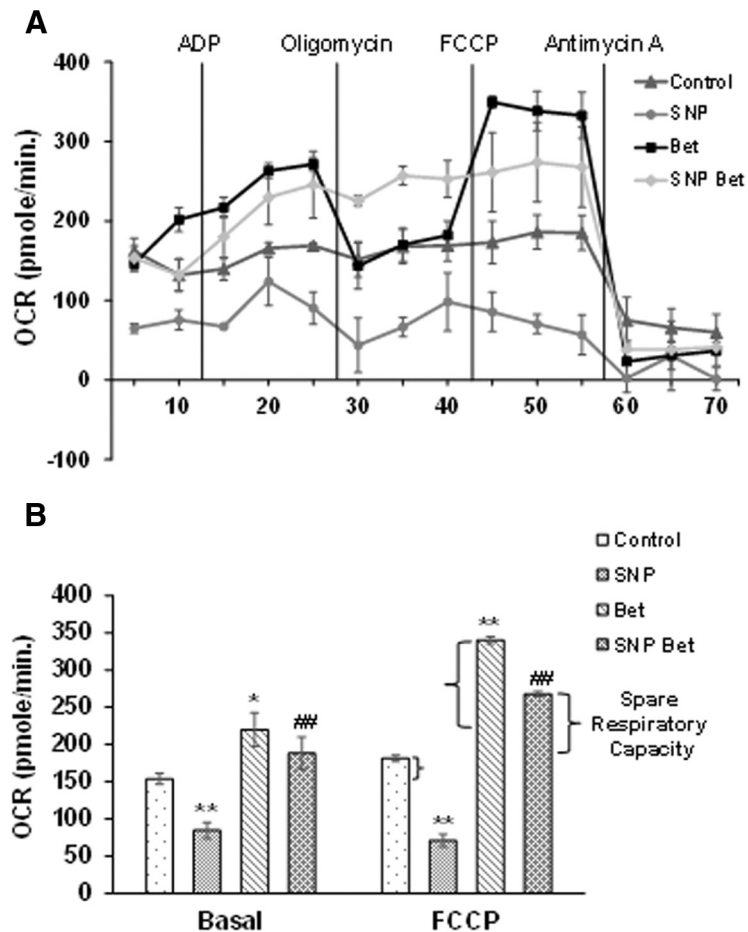


Figure 9. Betaine rescues SNP-mediated inhibition of mitochondrial respiration in SH-SY5Y cells. **A**, Respirometry traces show OCRs from mitochondria isolated from control SH-SY5Y cells and cells treated with 400 μ M SNP, 1 mM betaine, or both 400 μ M SNP/1 mM betaine. **B**, Quantitation of basal respiration and maximal respiratory capacity (after addition of the uncoupler FCCP) were determined for mitochondria isolated from control SH-SY5Y cells and cells treated with 400 μ M SNP, 1 mM betaine, and both SNP and betaine. Brackets represent spare respiratory capacity for control, betaine, and SNP/betaine-treated cell mitochondria. * $p < 0.05$ versus control. ** $p < 0.01$ versus control. ## $p < 0.01$ SNP-treated cells.

sured respiration (OCR) in mitochondria isolated from SH-SY5Y cells treated with either 400 μ M SNP or 1 mM betaine, or both 400 μ M SNP and 1 mM betaine for 20 h as shown in Figure 9. Basal respiration and maximal respiratory capacity (after addition of the uncoupler FCCP) were measured. These data show that SNP reduced respiration by >50% compared with control cells (Fig. 9A,B). Betaine treatment rescued basal respiration and maximal respiratory capacity in SNP-treated cell mitochondria, however, increasing basal respiration by 2.2-fold and maximal respiration by 1.4-fold (Fig. 9B). Betaine also increased spare respiratory capacity 2.9-fold in SNP/betaine-treated cells over SNP-treated cells and by 4.2-fold in betaine-treated cells compared with control SH-SY5Y cells (Fig. 9B, brackets). Spare respiratory capacity is a measure of a cell's ability to meet energetic demands; and in isolated mitochondria, it is related to the number of respiratory complexes per mitochondria. The increase in spare respiratory capacity as a result of betaine treatment in both SNP-treated and control cells suggests that betaine may not only act by maintaining H3K4me3 levels under oxidative conditions, but also by increasing the expression of respiratory complexes through a separate mechanism.

To understand whether betaine could regulate transcription in the absence of an inflammatory environment, we exploited the fact

that H3K4me3 marks many actively transcribed genes. We performed ChIP-seq with an antibody to H3K4me3 and chromatin isolated from control SH-SY5Y cells and cells treated with betaine. Although betaine did not significantly increase H3K4me3 in control SH-SY5Y cells (Fig. 8), it did increase spare respiratory capacity (Fig. 9), suggesting that expression of mitochondrial oxidative phosphorylation genes was increased. By performing ChIP-seq on chromatin from betaine-treated cells, genes actively transcribed should contain peaks for H3K4me3. After normalization to input DNA, our ChIP-seq analysis identified 3675 genes enriched for H3K4me3 peaks at least twofold in betaine ChIP DNA over control ChIP DNA. Enriched peaks within 20 kb of TSS or within genic regions were assigned to functional groups with PANTHER (<http://pantherdb.org/>). This analysis showed that 39% of genes enriched by ChIP-seq in cells treated with betaine were involved in cellular metabolism and 229 were located in mitochondria (Fig. 10A). Visualization of H3K4me3 peak enrichment with Strand NGS 2.5 software is shown in Figure 10B for select genes. In Figure 10B, the number of sequence reads are shown for input DNA, control ChIP DNA, and betaine ChIP DNA. The scale for the y -axis values denoting number of sequence reads are variable, so approximate numbers of reads are shown for each condition. We found that H3K4me3 peaks were enriched in sequences near the TSS or in genic/intronic regions of mitochondrial genes, including 41 subunit genes of the electron transport chain machinery. Table 4 shows genes with H3K4me3 enrichment with betaine treatment.

The chromosomal location, p values, Q scores, gene symbols, transcript accession numbers, regions that overlap with peaks (upstream, genic, or intron), and distance to the TSS for the nearest peak are shown for electron transport chain subunit genes and for mitochondrial transcription factors in Table 4. Genes with H3K4me3 enrichment included 21 subunits for Complex I (NADH dehydrogenase), two subunits for Complex III (ubiquinol cytochrome c oxidoreductase), 12 subunits for Complex IV (cytochrome oxidase), and 6 subunits for Complex V (ATP synthase). H3K4me3 was also enriched near the TSS or in genic/intronic regions of mitochondrial transcription factors, including nuclear respiratory factor 1 (*NRF1*), mitochondrial transcription factor A, and the estrogen-related receptor β (*ERR β*) and gamma (*ERR γ*) genes, which are nuclear receptors involved in regulating transcription of genes involved in energy homeostasis (Huss et al., 2015) (Table 4). To confirm gene expression changes as a result of betaine treatment, we performed qRT-PCR for a subset of genes in control, SNP treated, betaine-treated, and in SNP/betaine-treated cells. These data confirm that betaine can rescue expression levels of mitochondrial genes after SNP treatment (Fig. 11). Of the 10 genes tested, six genes, including components of the electron transport machinery *NDUFS4*, cytochrome c oxidase subunit Va (*COX5A*), cytochrome oxidase assembly homolog (*COX16*), ATP synthase subunit B1 (*ATP5F1*), and the

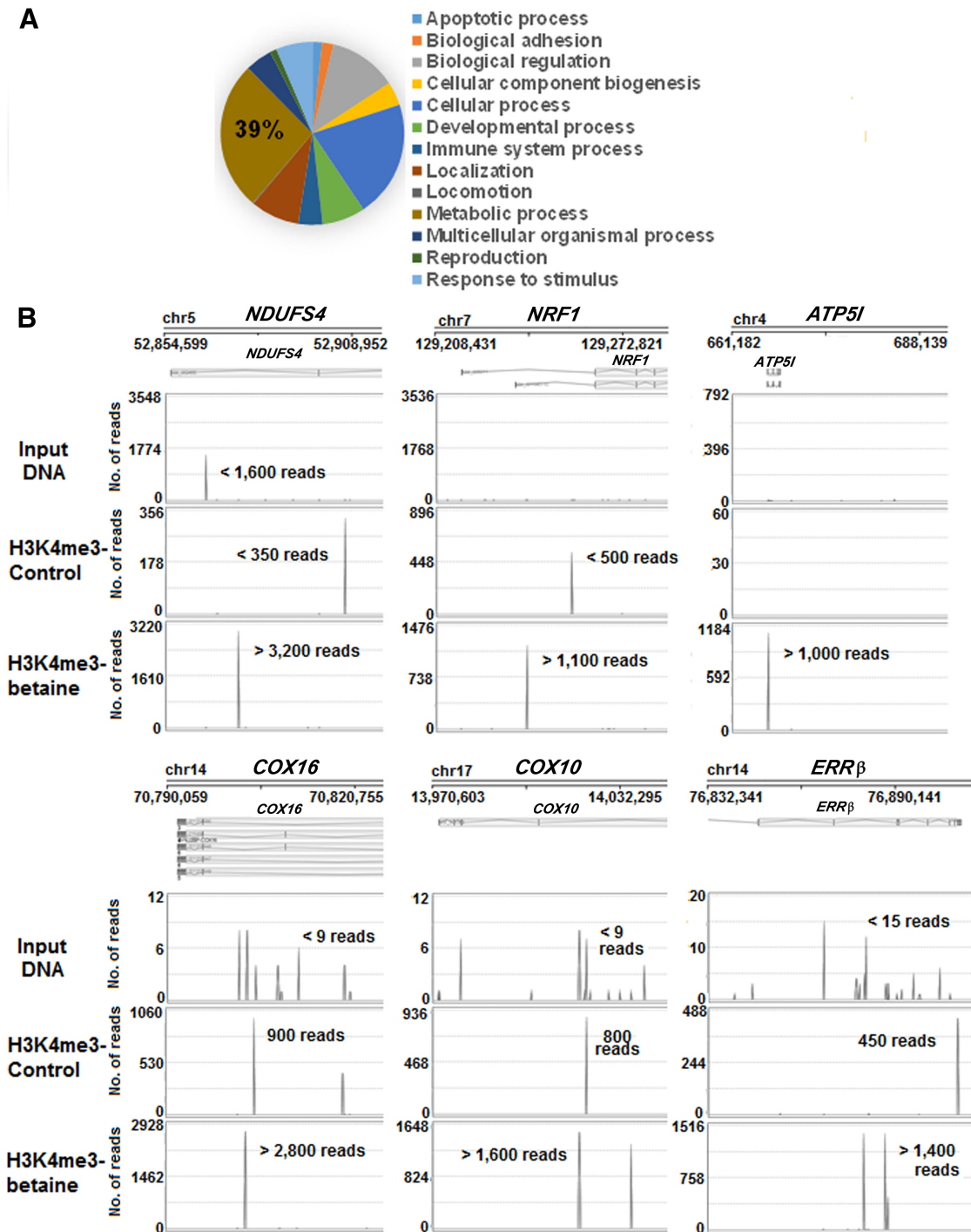


Figure 10. H3K4me3 peaks enriched by betaine treatment overlap with many mitochondrial genes. **A**, The 3675 genes enriched by ChIP-seq with an antibody to H3K4me3 after betaine treatment were assigned to functional groups (<http://pantherdb.org/>). A total of 39% were involved in cellular metabolism. **B**, Visualization of H3K4me3 peaks was performed with Strand NGS 2.5 software after peak identification with the Model-based Analysis of Chip-Seq algorithm. Chromosomal location and number of sequence reads are shown for control and betaine-treated ChIP DNA and for input DNA. Chromosomal regions enriched for H3K4me3 due to betaine treatment are shown for *NDUFS4*, *NRF1*, *ATP5I*, *COX16*, *COX10*, and *ERRβ*. The position of the transcripts and alternatively spliced variants for each gene relative to H3K4me3 peaks are shown. The scale of the y-axis denoting number of sequence reads is variable, so approximate sequence reads are shown next to the highest H3K4me3 peak in each panel.

transcriptional regulators *ERRγ* and *NRF1* were sensitive to redox dysregulation by SNP treatment, and expression levels were reversed with betaine (Fig. 11). We also found that betaine increased transcript levels for mitochondrial genes that were not repressed by SNP. Interestingly, these data also show that for several of the genes tested, expression was significantly enhanced with SNP and betaine treatment over betaine treatment alone (*UQCRC2*, *COX5A*, *ATP5F1*). As

a negative control, we also measured expression of the peroxisome proliferator-activated receptor gamma coactivator 1 α (*PPARGC1A*) gene, which is a transcriptional coactivator and mitochondrial biogenesis factor (Wu et al., 1999). The *PPARGC1A* gene contained H3K4me3 peaks that were enriched in control SH-SY5Y cells over input DNA (data not shown) but were not enriched by betaine. qRT-PCR confirmed the ChIP-seq data and

Table 4. Mitochondrial genes enriched for H3K4me3 after betaine treatment

Chromosome	Start	End	p value	Q score	Gene symbol	Longest transcript	Overlap type	Distance to TSS
chr1	161181309	161181359	5.8E-06	0.002	NDUFS2	NM_004550	Intron	12229
chr1	39490993	39491043	5.8E-06	0.002	NDUFS5	NM_004552	Upstream	−949
chr1	111992311	111992361	5.8E-06	0.002	ATP5F1	NM_001688	Intron	593
chr1	217299958	217300008	5.8E-06	0.002	ESRRG (ERR γ)	NM_001134285	Intron	11114
chr2	37463762	37463812	5.8E-06	0.002	NDUFAF7	NM_144736	Intron	5013
chr2	206996739	206996789	5.8E-06	0.002	NDUFS1	NM_001199983	Intron	27479
chr2	42592390	42592440	5.8E-06	0.002	COX7A2L	NM_004718	Upstream	−4059
chr3	120316387	120316437	5.8E-06	0.002	NDUFB4	NM_001168331	Intron	1284
chr3	48644850	48644900	5.8E-06	0.002	UQCRC1	NM_003365	Intron	2223
chr4	140214122	140214172	5.8E-06	0.002	NDUFC1	NM_001184988	Intron	9558
chr4	46912869	46912919	5.8E-06	0.002	COX7B2	NM_130902	Upstream	−1642
chr4	666439	666489	5.8E-06	0.002	ATP5I	NM_007100	Intron	1663
chr5	60254967	60255017	5.8E-06	0.002	NDUFAF2	NM_174889	Intron	14036
chr5	52875692	52875743	8E-09	1E-05	NDUFS4	NM_002495	Intron	19252
chr7	123197493	123197543	5.8E-06	0.002	NDUFA5	NM_005000	CDS-Exon, Intron	440
chr7	1015028	1015078	5.8E-06	0.002	COX19	NM_001031617	CDS-Exon, Intron	182
chr7	99023956	99024006	5.8E-06	0.002	ATP5J2	NM_001198879	Intron	39843
chr7	129261774	129261824	5.8E-06	0.002	NRF1	NM_005011	Intron	10244
chr8	96039143	96039193	5.8E-06	0.002	NDUFAF6	NM_152416	Intron	1954
chr8	100898116	100898166	5.8E-06	0.002	COX6C	NM_004374	Intron	8101
chr9	32567493	32567543	5.8E-06	0.002	NDUFB6	NM_001199987	Intron	5664
chr10	101482899	101482949	5.8E-06	0.002	COX15	NM_078470	Intron	9499
chr10	60148120	60148170	5.8E-06	0.002	TFAM	NM_003201	Intron	3242
chr11	77771397	77771447	5.8E-06	0.002	NDUFC2	NM_001203262	Intron	19843
chr11	47598422	47598472	5.8E-06	0.002	NDUFS3	NM_004551	Upstream	−2115
chr11	67375221	67375271	5.8E-06	0.002	NDUFV1	NM_007103	Intron	923
chr12	95399283	95399355	8E-09	1E-05	NDUFA12	NM_018838	Upstream	−1830
chr12	54067324	54067374	5.8E-06	0.002	ATP5G2	NM_001002031	Intron	3163
chr14	92582652	92582702	5.8E-06	0.002	NDUFB1	NM_004545	Intron	5476
chr14	70811575	70811625	5.8E-06	0.002	COX16	NM_001204090	Intron	14848
chr14	50779994	50780044	5.8E-06	0.002	ATP5S	NR_033761	Intron	972
chr14	76857369	76857419	5.8E-06	0.002	ESRRB (ERR β)	NM_004452	Intron	31692
chr16	21977385	21977435	5.8E-06	0.002	UQCRC2	NM_003366	Intron	12801
chr16	85838085	85838135	5.8E-06	0.002	COX4I1	NM_001861	Intron	4937
chr16	31441644	31441694	5.8E-06	0.002	COX6A2	NM_005205	Upstream	−1920
chr17	14035990	14036040	5.8E-06	0.002	COX10	NM_001303	Intron	63296
chr17	13964251	13964301	5.8E-06	0.002	COX10-AS1	NR_049718	Intron	8499
chr17	53038289	53038339	5.8E-06	0.002	COX11	NR_027942	Intron	7750
chr19	8389711	8389761	5.8E-06	0.002	NDUFA7	NM_005001	Upstream	−3456
chr19	14681231	14681281	5.8E-06	0.002	NDUFB7	NM_004146	Intron	1633
chr19	36644626	36644676	5.8E-06	0.002	COX7A1	NM_001864	Upstream	−880
chr20	13777570	13777620	5.8E-06	0.002	NDUFAF5	NM_024120	Intron	11923
chr21	44315463	44315513	5.8E-06	0.002	NDUFV3	NM_001001503	Intron	2110
chr21	27105277	27105327	5.8E-06	0.002	ATP5J	NM_001685	Intron	2663
chr22	42495549	42495599	5.8E-06	0.002	NDUFA6-AS1	NR_034118	Intron	8637

shows that *PPARGC1A* expression was not increased in betaine-treated cells (Fig. 11).

Discussion

In an effort to understand epigenetic mechanisms involved in cortical mitochondrial changes in MS, we measured concentrations of methionine cycle metabolites, histone H3 methylation patterns, and markers of oxidative phosphorylation in MS cortical gray matter samples compared with controls. In contrast to methionine metabolite changes reported in MS sera and plasma, including decreased methionine and B₁₂, and increased homocysteine, we found significantly decreased concentrations of cystathionine, SAM, and betaine in MS cortical samples. Cystathionine is a substrate in the transsulfuration pathway, which generates the redox regulator GSH. Decreased cystathionine in MS is indicative of an imbalance in redox homeostasis and is consistent with studies demonstrating increased oxidative damage in the MS brain due to activated microglial derived NO and ROS

(Gilgun-Sherki et al., 2004; Gonsette, 2008; Pandit et al., 2009). We also found reductions in levels of mitochondrial electron transport chain complexes and decreased concentrations of the neuronal mitochondrial metabolite NAA, which is linked to ATP production and mitochondrial oxidative phosphorylation (Clark, 1998; Li et al., 2013), in MS samples. NAA levels were found to be correlated with cystathionine concentration, suggesting that there is a relationship between dysregulation of redox homeostasis and neuronal respiratory capacity in MS.

The methyl donors SAM and betaine were also reduced in MS cortical gray matter. Decreased availability of these methyl donors in MS could impact methylation of DNA and histones, chromatin conformation, and gene expression. Decreasing SAM concentration in stem cell cultures has been shown to result in changes in histone H3 methylation patterns (Shyh-Chang et al., 2013). Betaine serves a dual role in cells as a methyl donor and in osmoregulation and regulation of cell volume (Lang, 2007). The

source of betaine is almost completely from dietary intake of betaine or choline, which can be oxidized in mitochondria by the enzyme choline dehydrogenase to generate betaine in some tissues. It has been established that betaine acts as a methyl donor in the liver and during development in the CNS. Dietary betaine supplementation has been shown to induce site-specific changes in DNA methylation in the liver in a mouse model of ethanol-induced liver damage (Medici et al., 2014). Other studies in rats have demonstrated that high maternal dietary choline can regulate expression of histone methyltransferases and histone H3 methylation patterns in the liver and brain in the developing fetus (Davison et al., 2009; Blusztajn and Mellott, 2012). This effect of choline on histone methylation is mediated by the BHMT pathway after conversion of choline to betaine. BHMT is expressed in the CNS during development but in the adult BHMT expression has been believed to be restricted primarily to the liver, kidney, and lens of the eye (Lever and Slow, 2010). Our data showing expression of BHMT in the adult CNS suggest that betaine may also supply methyl groups to remethylate homocysteine to methionine in place of 5-methyltetrahydrofolate in adult brain tissue and in neurons in some circumstances. This would explain our findings, which show a correlation between betaine and H3K4me3 in postmortem cortical tissue and regulation of H3K4me3 levels by betaine in neuroblastoma cells. Consistent with our results, other studies investigating homocysteine metabolism support a role for betaine as a methyl donor in the CNS. In a study by Zhang et al. (2013), BHMT expression was reported in the brain of bats during hibernation. The authors concluded that BHMT remethylated homocysteine to methionine with betaine as the methyl donor to prevent toxic buildup of homocysteine during long periods of hibernation when nutrients, including vitamin B₁₂, which are essential for methionine synthase activity are depleted. In another study, dietary betaine supplementation was found to improve memory in a rat model of hyperhomocysteinemia (Chai et al., 2013). In this rat model, betaine appeared to provide neuroprotection by preventing the accumulation of homocysteine, which can be toxic to neurons by supplying methyl groups to remethylate homocysteine to methionine.

Increased dietary betaine and choline intake has been shown to be correlated with decreases in inflammatory markers, including C-reactive protein, proinflammatory cytokines, and homocysteine (Detopoulou et al., 2008), suggesting that decreased betaine concentrations in MS may contribute to and exacerbate

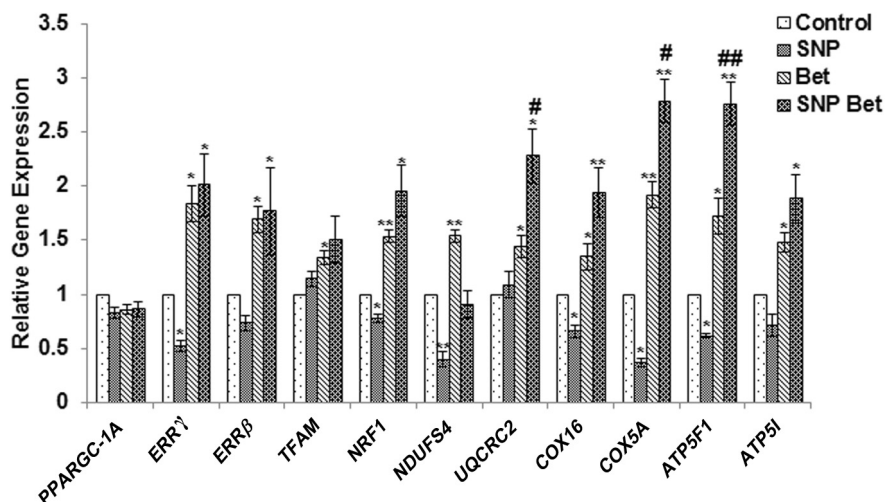


Figure 11. Betaine increases expression of mitochondrial genes. Changes in gene expression were confirmed by qRT-PCR for select transcripts showing enrichment for H3K4me3 as a result of betaine treatment. qRT-PCR was performed with RNA isolated from control SH-SY5Y cells and cells treated with SNP, betaine, or SNP/betaine. Relative expression levels with controls set at 1 are shown. Error bars indicate SEM. **p* < 0.05 versus control. ***p* < 0.01 versus control. #*p* < 0.05 versus betaine-treated cells. ##*p* < 0.01 versus betaine-treated cells.

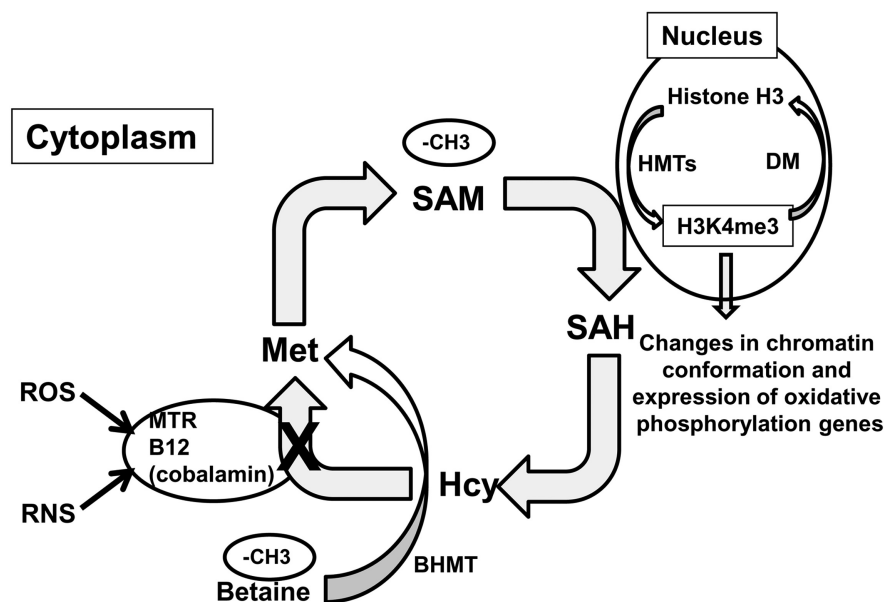


Figure 12. Schematic represents the relationship between methionine metabolism and mitochondrial changes in MS cortex. Inflammation in MS leads to increased ROS and RNS, which may inhibit the B₁₂-dependent MTR reaction. Inhibition of methionine synthase can be overcome by activation of the BHMT–betaine pathway to remethylate homocysteine (Hcy) to methionine (Met). Depletion of the methyl donor betaine in MS cortical gray matter may lead to an inability to overcome the inhibition of methionine synthase that would result in decreases in levels of the methyl donor SAM and decreased H3K4me3. The H3K4me3 histone methyl mark activates transcription of oxidative phosphorylation genes, which are decreased in MS. HMT, Histone methyltransferases; DM, demethylases; –CH₃, methyl groups supplied by betaine and SAM.

oxidative damage already present in the MS brain. It has been demonstrated that the activity of methionine synthase is sensitive to changes in redox homeostasis. The transient cob(I)alamin form of holo methionine synthase is sensitive to oxidation by NO (Nicolaou et al., 1994, 1996; Jarrett et al., 1998; Danishpajooch et al., 2001; Mukherjee and Brasch, 2011) and is inhibited when oxidized. Increased NO and reactive nitrogen species (RNS) in the MS brain may lead to oxidation and inhibition of methionine synthase. Our data suggest that, under these conditions, the methionine synthase reaction could be circumvented and homocys-

teine could be remethylated to methionine in the CNS by the activity of BHMT with betaine supplying the methyl groups. The cause for decreased betaine in the MS brain is not clear but could result from either dietary deficiency or loss due to diffusion out of demyelinated axons to counteract cell swelling and resulting changes in osmolarity. In any case, depletion of betaine in MS would leave cells unable to compensate for inhibition of methionine synthase through the BHMT pathway under oxidative conditions (Fig. 12). If this were the case, we would expect that homocysteine would be increased. Consistent with this explanation, we found that homocysteine and SAM were negatively correlated ($r = -0.3, p = 0.04$).

Studies analyzing postmortem tissue as well as *in vivo* magnetic resonance spectroscopy studies have implicated mitochondrial impairment in MS cortical pathology. These mitochondrial changes may be detrimental in MS by limiting the supply of ATP necessary for neurons to regulate ion homeostasis, vesicular transport, and other energy-dependent processes. Indeed, studies have indicated that defects in neuronal respiration precede neurodegeneration in MS (Ge et al., 2004; Cader et al., 2007). The present study suggests that a novel mechanism involving dysregulation of methionine metabolism contributes to mitochondrial impairment in MS. This may explain the observed overlap in pathological changes, which occur in B₁₂ deficiency and in MS (Miller et al., 2005). Our analysis of MS and control postmortem cortical tissue suggests that inadequate betaine concentrations in the MS brain may leave cells unable to compensate for the inhibitory effects of an inflammatory environment on methionine synthase activity and may result in dysregulation of methionine metabolism and reduced levels of H3K4me3 (Fig. 12). This mechanism is supported by our cell culture data. These data show that the BHMT–betaine pathway does indeed appear to provide a mechanism to maintain methionine metabolism under the type of oxidative and inflammatory conditions that exist in MS. We found that exposing SH-SY5Y neuroblastoma cells to the NO donor SNP leads to reductions in H3K4me3 levels, expression of some mitochondrial genes, and mitochondrial respiration. Treatment with betaine reverses these effects and results in increased mitochondrial respiratory capacity. These data are consistent with another recent report, which showed that betaine increased respiration and cytochrome oxidase expression in a liver cell line (Lee, 2015).

Our CHIP-seq data also suggest that, in addition to maintaining expression of mitochondrial genes by reversing the effects of RNS on H3K4me3 levels, betaine can also activate expression of mitochondrial genes under normal physiological conditions. Genes with H3K4me3 enrichment indicating that they were actively transcribed with betaine treatment included mitochondrial transcriptional activators *ERRβ*, *ERRγ*, *NRF1*, mitochondrial transcription factor A, and many mitochondrial oxidative phosphorylation genes. Our data indicate that the expression levels of some genes with H3K4me3 enrichment as a result of betaine treatment, including *ERRγ*, *NRF1*, *NDUFS4*, *COX5A*, *COX16*, and *ATP5F1*, were decreased by SNP potentially as a consequence of decreased H3K4me3 levels. Although betaine rescued expression of these genes after SNP treatment, it also increased expression levels of all of the genes tested in the absence of SNP, when H3K4me3 levels would not be altered. This suggests that the BHMT–betaine pathway may also act through additional mechanisms by modifying methylation of other histone sites and/or DNA. However, our qRT-PCR data also show that expression was enhanced with SNP and betaine treatment over betaine treatment alone. A possible explanation for this observation could be

that BHMT activity may increase with redox dysregulation. If this were the case, we would have expected that, in our respirometry experiments, spare respiratory capacity would be higher in SNP/betaine-treated cells compared with betaine alone, but this was not the case. Although spare respiratory capacity was increased in SNP/betaine-treated cells over controls, it was not as high as in betaine-treated cells. This could be due to other effects of NO in cells, however, such as nitration and inhibition of respiratory complexes (Sarti et al., 2003).

Our data demonstrate that decreased betaine in MS cortex is correlated with altered methylation of H3K4me3 and may contribute to decreased expression of oxidative phosphorylation genes and respiratory defects in MS cortex. These data indicate that dietary betaine supplementation may support mitochondrial respiration and provide neuroprotection in MS.

References

- Bjartmar C, Kidd G, Mörk S, Rudick R, Trapp BD (2000) Neurological disability correlates with spinal cord axonal loss and reduced N-acetylaspartate in chronic multiple sclerosis patients. *Ann Neurol* 48:893–901. [CrossRef Medline](#)
- Blusztajn JK, Mellott TJ (2012) Choline nutrition programs brain development via DNA and histone methylation. *Cent Nerv Syst Agents Med Chem* 12:82–94. [CrossRef Medline](#)
- Bö L, Geurts JJ, Mörk SJ, van der Valk P (2006) Grey matter pathology in multiple sclerosis. *Acta Neurol Scand Suppl* 183:48–50. [Medline](#)
- Börsch-Haubold AG, Montero I, Konrad K, Haubold B (2014) Genome-wide quantitative analysis of histone h3 lysine 4 trimethylation in wild house mouse liver: environmental change causes epigenetic plasticity. *PLoS One* 9:e97568. [CrossRef Medline](#)
- Broadwater L, Pandit A, Azzam S, Clements R, Vadnal J, Sulak M, Yong VW, Freeman EJ, Gregory RB, McDonough J (2011) Analysis of the mitochondrial proteome in multiple sclerosis cortex. *Biochim Biophys Acta* 1812:630–641. [CrossRef Medline](#)
- Cader S, Johansen-Berg H, Wylezinska M, Palace J, Behrens TE, Smith S, Matthews PM (2007) Discordant white matter N-acetylaspartate and diffusion MRI measures suggest that chronic metabolic dysfunction contributes to axonal pathology in multiple sclerosis. *Neuroimage* 36:19–27. [CrossRef Medline](#)
- Campbell GR, Ziabreva I, Reeve AK, Krishnan KJ, Reynolds R, Howell O, Lassmann H, Turnbull DM, Mahad DJ (2011) Mitochondrial DNA deletions and neurodegeneration in multiple sclerosis. *Ann Neurol* 69:481–492. [CrossRef Medline](#)
- Chai GS, Jiang X, Ni ZF, Ma ZW, Xie AJ, Cheng XS, Wang Q, Wang JZ, Liu GP (2013) Betaine attenuates Alzheimer-like pathological changes and memory deficits induced by homocysteine. *J Neurochem* 124:388–396. [CrossRef Medline](#)
- Clark JB (1998) N-acetyl aspartate: a marker for neuronal loss or mitochondrial dysfunction. *Dev Neurosci* 20:271–276. [CrossRef Medline](#)
- Cyr AR, Domann FE (2011) The redox basis of epigenetic modifications: from mechanisms to functional consequences. *Antioxid Redox Signal* 15:551–589. [CrossRef Medline](#)
- Danishpajoo IO, Gudi T, Chen Y, Kharitonov VG, Sharma VS, Boss GR (2001) Nitric oxide inhibits methionine synthase activity *in vivo* and disrupts carbon flow through the folate pathway. *J Biol Chem* 276:27296–27303. [CrossRef Medline](#)
- Davison JM, Mellott TJ, Kovacheva VP, Blusztajn JK (2009) Gestational choline supply regulates methylation of histone H3, expression of histone methyltransferases G9a (Kmt1c) and Suv39h1 (Kmt1a), and DNA methylation of their genes in rat fetal liver and brain. *J Biol Chem* 284:1982–1989. [CrossRef Medline](#)
- Detopoulou P, Panagiotakos DB, Antonopoulou S, Pitsavos C, Stefanadis C (2008) Dietary choline and betaine intakes in relation to concentrations of inflammatory markers in healthy adults: the ATTICA study. *Am J Clin Nutr* 87:424–430. [Medline](#)
- Dutta R, McDonough J, Yin X, Peterson J, Chang A, Torres T, Guduz T, Macklin WB, Lewis DA, Fox RJ, Rudick R, Mirnic K, Trapp BD (2006) Mitochondrial dysfunction as a cause of axonal degeneration in multiple sclerosis patients. *Ann Neurol* 59:478–489. [CrossRef Medline](#)
- Fisher E, Lee JC, Nakamura K, Rudick RA (2008) Gray matter atrophy in

- multiple sclerosis: a longitudinal study. *Ann Neurol* 64:255–265. [CrossRef Medline](#)
- Frost B, Hemberg M, Lewis J, Feany MB (2014) Tau promotes neurodegeneration through global chromatin relaxation. *Nat Neurosci* 17:357–366. [CrossRef Medline](#)
- Fuso A, Nocolia V, Cavallaro RA, Scarpa S (2011a) DNA methylase and demethylase activities are modulated by one-carbon metabolism in Alzheimer's disease models. *J Nutr Biochem* 22:242–251. [CrossRef Medline](#)
- Fuso A, Nocolia V, Pasqualato A, Fiorenza MT, Cavallaro RA, Scarpa S (2011b) Changes in Presenilin 1 gene methylation pattern in diet-induced B vitamin deficiency. *Neurobiol Aging* 32:187–199. [CrossRef Medline](#)
- Gardner LA, Desiderio DM, Groover CJ, Hartzes A, Yates CR, Zucker-Levin AR, Bloom L, Levin MC (2013) LC-MS/MS identification of the one-carbon cycle metabolites in human plasma. *Electrophoresis* 34:1710–1716. [CrossRef Medline](#)
- Ge Y, Gonen O, Inglese M, Babb JS, Markowitz CE, Grossman RI (2004) Neuronal cell injury precedes brain atrophy in multiple sclerosis. *Neurology* 62:624–627. [CrossRef Medline](#)
- Gilgun-Sherki Y, Melamed E, Offen D (2004) The role of oxidative stress in the pathogenesis of multiple sclerosis: the need for effective antioxidant therapy. *J Neurol* 251:261–268. [CrossRef Medline](#)
- Gonsette RE (2008) Neurodegeneration in multiple sclerosis: the role of oxidative stress and excitotoxicity. *J Neurol Sci* 274:48–53. [CrossRef Medline](#)
- Huss JM, Garbacz WG, Xie W (2015) Constitutive activities of estrogen-related receptors: transcriptional regulation of metabolism by the ERR pathways in health and disease. *Biochim Biophys Acta* 1852:1912–1927. [CrossRef Medline](#)
- Huynh JL, Garg P, Thin TH, Yoo S, Dutta R, Trapp BD, Haroutunian V, Zhu J, Donovan MJ, Sharp AJ, Casaccia P (2014) Epigenome-wide differences in pathology-free regions of multiple sclerosis-affected brains. *Nat Neurosci* 17:121–130. [CrossRef Medline](#)
- Inglese M, Ge Y, Filippi M, Falini A, Grossman RI, Gonen O (2004) Indirect evidence for early widespread gray matter involvement in relapsing-remitting multiple sclerosis. *Neuroimage* 21:1825–1829. [CrossRef Medline](#)
- Inoue-Choi M, Nelson HH, Robien K, Arning E, Bottiglieri T, Koh WP, Yuan JM (2013) Plasma S-adenosylmethionine, DNMT polymorphisms, and peripheral blood LINE-1 methylation among healthy Chinese adults in Singapore. *BMC Cancer* 13:389. [CrossRef Medline](#)
- Jarrett JT, Huang S, Matthews RG (1998) Methionine synthase exists in two distinct conformations that differ in reactivity toward methyltetrahydrofolate, adenosylmethionine, and flavodoxin. *Biochemistry* 37:5372–5382. [CrossRef Medline](#)
- Kocer B, Engur S, Ak F, Yilmaz M (2009) Serum vitamin B12, folate, and homocysteine levels and their association with clinical and electrophysiological parameters in multiple sclerosis. *J Clin Neurosci* 16:399–403. [CrossRef Medline](#)
- Lang F (2007) Mechanisms and significance of cell volume regulation. *J Am Coll Nutr* 26 [Suppl 5]:613S–623S.
- Lee I (2015) Betaine is a positive regulator of mitochondrial respiration. *Biochem Biophys Res Commun* 456:621–625. [CrossRef Medline](#)
- Lever M, Slow S (2010) The clinical significance of betaine, an osmolyte with a key role in methyl group metabolism. *Clin Biochem* 43:732–744. [CrossRef Medline](#)
- Li S, Clements R, Sulak M, Gregory R, Freeman E, McDonough J (2013) Decreased NAA in gray matter is correlated with decreased availability of acetate in white matter in postmortem multiple sclerosis cortex. *Neurochem Res* 38:2385–2396. [CrossRef Medline](#)
- Mastronardi FG, Noor A, Wood DD, Paton T, Moscarello MA (2007) Peptidyl argininedeiminase 2 CpG island in multiple sclerosis white matter is hypomethylated. *J Neurosci Res* 85:2006–2016. [CrossRef Medline](#)
- Medici V, Schroeder DI, Woods R, LaSalle JM, Geng Y, Shibata NM, Peerson J, Hodzic E, Dayal S, Tsukamoto H, Kharbanda KK, Tillman B, French SW, Halsted CH (2014) Methylation and gene expression responses to ethanol feeding and betaine supplementation in the cystathionine beta synthase-deficient mouse. *Alcohol Clin Exp Res* 38:1540–1549. [CrossRef Medline](#)
- Mehler MF (2008) Epigenetics and the nervous system. *Ann Neurol* 64:602–617. [CrossRef Medline](#)
- Miller A, Korem M, Almog R, Galboiz Y (2005) Vitamin B12, demyelination, remyelination and repair in multiple sclerosis. *J Neurol Sci* 233:93–97. [CrossRef Medline](#)
- Mukherjee R, Brasch NE (2011) Kinetic studies on the reaction between cob(I)alamin and peroxyxynitrite: rapid oxidation of cob(I)alamin to cob(II)alamin by peroxyxynitrous acid. *Chemistry* 17:11723–11727. [CrossRef Medline](#)
- Nicolaou A, Ast T, Velasco Garcia CV, Anderson MM, Gibbons JM, Gibbons WA (1994) In vitro NO and N2O inhibition of the branch point enzyme vitamin B12 dependent methionine synthase from rat brain synaptosomes. *Biochem Soc Trans* 22:296S. [CrossRef Medline](#)
- Nicolaou A, Kenyon SH, Gibbons JM, Ast T, Gibbons WA (1996) In vitro inactivation of mammalian methionine synthase by nitric oxide. *Eur J Clin Invest* 26:167–170. [CrossRef Medline](#)
- Noseworthy JH, Lucchinetti C, Rodriguez M, Weinshenker BG (2000) Multiple sclerosis. *N Engl J Med* 343:938–952. [CrossRef Medline](#)
- Pandit A, Vadnal J, Houston S, Freeman E, McDonough J (2009) Impaired regulation of electron transport chain subunit genes by nuclear respiratory factor 2 in multiple sclerosis. *J Neurol Sci* 279:14–20. [CrossRef Medline](#)
- Pedre X, Mastronardi F, Bruck W, López-Rodas G, Kuhlmann T, Casaccia P (2011) Changed histone acetylation patterns in normal-appearing white matter and early multiple sclerosis lesions. *J Neurosci* 31:3435–3445. [CrossRef Medline](#) Erratum in: *J Neurosci* 31:8325.
- Reynolds EH, Bottiglieri T, Laundry M, Crellin RF, Kirker SG (1992) Vitamin B12 metabolism in multiple sclerosis. *Arch Neurol* 49:649–652. [CrossRef Medline](#)
- Sandstrom RS, Foret MR, Grow DA, Haugen E, Rhodes CT, Cardona AE, Phelix CF, Wang Y, Berger MS, Lin CH (2014) Epigenetic regulation by chromatin activation mark H3K4me3 in primate progenitor cells within adult neurogenic niche. *Sci Rep* 4:5371. [CrossRef Medline](#)
- Sarti P, Giuffrè A, Barone MC, Forte E, Mastronicola D, Brunori M (2003) Nitric oxide and cytochrome oxidase: reaction mechanisms from the enzyme to the cell. *Free Radic Biol Med* 34:509–520. [CrossRef Medline](#)
- Shyh-Chang N, Locasale JW, Lyssiotis CA, Zheng Y, Teo RY, Ratanasirintra-woot S, Zhang J, Onder T, Unternaehrer JJ, Zhu H, Asara JM, Daley GQ, Cantley LC (2013) Influence of threonine metabolism on S-adenosylmethionine and histone methylation. *Science* 339:222–226. [CrossRef Medline](#)
- Witte ME, Nijland PG, Drexhage JA, Gerritsen W, Geerts D, van Het Hof B, Reijerkerk A, de Vries HE, van der Valk P, van Horsen J (2013) Reduced expression of PGC-1 α partly underlies mitochondrial changes and correlates with neuronal loss in multiple sclerosis cortex. *Acta Neuropathol* 125:231–243. [CrossRef Medline](#)
- Wu Z, Puigserver P, Andersson U, Zhang C, Adelmant G, Mootha V, Troy A, Cinti S, Lowell B, Scarpulla RC, Spiegelman BM (1999) Mechanisms controlling mitochondrial biogenesis and respiration through the thermogenic coactivator PGC-1. *Cell* 98:115–124. [CrossRef Medline](#)
- Zhang Y, Liu T, Meyer CA, Eeckhoutte J, Johnson DS, Bernstein BE, Nusbaum C, Myers RM, Brown M, Li W, Liu XS (2008) Model-based analysis of ChIP-Seq (MACS). *Genome Biol* 9:R137. [CrossRef Medline](#)
- Zhang Y, Zhu T, Wang L, Pan YH, Zhang S (2013) Homocysteine homeostasis and betaine-homocysteine S-methyltransferase expression in the brain of hibernating bats. *PLoS One* 8:e85632. [CrossRef Medline](#)
- Zhu Y, He ZY, Liu HN (2011) Meta-analysis of the relationship between homocysteine, vitamin B₁₂, folate, and multiple sclerosis. *J Clin Neurosci* 18:933–938. [CrossRef Medline](#)